Rapid simulation of wave runup on morphologically diverse, reef-lined coasts with the BEWARE-2 meta-process model

Robert McCall[1], Curt Storlazzi[2], Floortje Roelvink[1], Stuart G. Pearson[3], Roel de Goede[1], and José A.Á. Antolínez[3]

[1]Deltares, Unit of Marine and Coastal Systems, Boussinesqweg 1, Delft, the Netherlands
[2]U.S. Geological Survey, Pacific Coastal and Marine Science Center, 2885 Mission St, Santa Cruz, California, United States of America
[3]Department of Hydraulic Engineering, Faculty of Civil Engineering and Geosciences, Delft University of Technology, Stevinweg 1, Delft, the Netherlands

Correspondence: Robert McCall (robert.mccall@deltares.nl)

Abstract. Low-lying, tropical coral reef-lined coastlines are becoming increasingly vulnerable to wave-driven flooding due to population growth, coral reef degradation, and sea-level rise. Early-warning systems (EWS) are needed to enable coastal authorities to issue timely alerts and coordinate preparedness and evacuation measures for their coastal communities. At longer time scales, risk management and adaptation planning require robust assessments of future flooding hazard considering uncertainties. However, due to diversity in reef morphologies and complex reef hydrodynamics compared to sandy shorelines, there have been no robust, analytical solutions for wave runup to allow the development of large-scale coastal wave-driven flooding EWS and risk assessment frameworks for reef-lined coasts. To address the need for fast, robust predictions of runup that account for the natural variability of coral reef morphologies, we constructed the BEWARE-2 (Broad-range Estimator of Wave Attack in Reef Environments) meta-process modeling system. We developed this meta-process model using a training dataset of hydrodynamics and wave runup computed by the XBeach Non-Hydrostatic+ process-based hydrodynamic model for 440 combinations of water level, wave height, and wave period, on 195 representative reef profiles that encompass the natural diversity in real-world fringing coral reef systems. Through this innovation, BEWARE-2 can be applied in a larger range of coastal settings than meta-models that rely on a parametric description of the coral reef geometry. In validation, the BEWARE-2 modeling system produced runup results that had a relative root-mean square error of 13% and relative bias of 5% relative to runup simulated by XBeach Non-Hydrostatic+ for a large range of oceanographic forcing conditions and for a diverse reef morphologies (root-mean square error and bias 0.63 m and 0.26 m, respectively, relative to mean simulated wave runup of 4.85 m). Incorporating parametric modifications in the modeling system to account for variations in reef roughness and beach slope allows systematic errors (relative bias) in BEWARE-2 predictions to be reduced by a factor of 1.5–6.5 for relatively coarse or smooth reefs, and mild or steep beach slopes. This prediction is provided by the BEWARE-2 modeling system 4–5 orders of magnitude faster than the full, process-based hydrodynamic model and could therefore be integrated in large-scale EWS for tropical, reef-lined coasts, as well as used for large-scale flood risk assessments.

1 Introduction

Low-lying, tropical coral reef-lined coastlines are vulnerable to wave-driven overwash and flooding. These flooding events will become more frequent as sea level rises due to climate-change (Vitousek et al., 2017; Vousdoukas et al., 2018), threatening infrastructure, ecosystems, and freshwater resources and infrastructure (Reynolds et al., 2015; Shimozono et al., 2015; Albert et al., 2016; Storlazzi et al., 2018). Globally, coral reefs protect more than 200,000 people living on the coast from flooding annually (Beck et al., 2018). These populations are denser, growing faster, and composed of more people from lower-middle income groups than the global average (Kumar and Taylor, 2015; Sing Wong et al., 2022). The combined increase in hazard probability and exposure is leading to a higher likelihood of flood-related deaths (Chilunga et al., 2017). This increased risk necessitates: 1) better science and understanding of flood risk drivers in the tropics; 2) better, locally-appropriate risk reduction and adaptation strategies to reduce coastal flooding and associated hazards (Hinkel et al., 2014); and 3) access to warning systems to increase preparedness and implement flood mitigation actions (Winter et al., 2020).

Short-term forecasts (typically up to 5–7 days) produced by EWS allow authorities to issue timely warnings and coordinate preparation and evacuation measures, which ultimately reduce risk to lives and assets. Events such as Typhoon Haiyan (Roeber and Bricker, 2015) and widespread flooding of islands due to remotely generated swell in the western Pacific (Hoeke et al., 2013; Wadey et al., 2017; Ford et al., 2018; Wandres et al., 2020; Hoeke et al., 2021) highlight the need for these warnings of impending coastal flooding events. One third of the world population live in areas that are not covered by EWS, with particularly low EWS coverage in least developed countries and small island developing states (WMO, 2022a). This issue has gained worldwide attention, and as a result the United Nations-endorsed Sendai Framework for Disaster Risk Reduction has called for improved access to early warning systems and disaster risk assessments by 2030 (UNISDR, 2015).

EWS have been implemented in sandy coastal environments (e.g., Doong et al., 2012; Coz et al., 2021; Stockdon et al., 2023), but reef-lined coasts demand different modeling approaches due to the complex bathymetry and wave dynamics characteristic of reef environments. Coral reef-lined (fringing reef) coasts are typically fronted by a shallow reef flat and a steeper fore reef farther offshore that dissipates open-ocean incoming wave energy through wave breaking and bottom friction (Lowe et al., 2005; Monismith et al., 2013). Wave breaking on the fore reef induces high radiation stress gradients, which results in significant wave-induced set-up on the reef flat (Pomeroy et al., 2012; Beck et al., 2018). Some of the dissipated incident-band (sea-swell; > 0.05 Hz) wave energy is transferred to infragravity-band ("IG," 0.005–0.05 Hz) and very low frequency-band waves ("VLF," 0.001–0.005 Hz) through breakpoint forcing (Symonds et al., 1982) on the steep fore reef (Péquignet et al., 2009; Pomeroy et al., 2012; Péquignet et al., 2014; Cheriton et al., 2016). Resonant amplification of IG and/or VLF waves can occur when their energy is concentrated at the natural frequency of the reef flat, which is most likely to occur on smooth reefs, with increasing water depth, high incident-band wave periods, and specific reef dimensions (Péquignet et al., 2009, 2014; Quataert et al., 2015; Gawehn et al., 2016; Pearson et al., 2017; Buckley et al., 2018). The complex interaction between tides, storm surge, wave-induced set-up, incident-band waves, IG waves, and VLF waves drives runup and subsequent flooding along reef-lined coasts.

55   Findings from sandy beach investigations are not necessarily transferable to coral reef-lined coasts. First, the bathymetric profiles of reef-lined coasts are starkly different from those of gently sloping beaches (Scott et al., 2020). Secondly, coral reefs can have much greater bed roughness, varying between the extremes of relatively smooth "pavement" reefs with little coral coverage to rough regimes with high coral coverage or/and bedrock rugosity (Quataert et al., 2015; Harris et al., 2018). Together, these severely limit the use of parametric models (e.g., Stockdon et al., 2006; Merrifield et al., 2014) in coral reef environments

60   (see also Astorga-Moar and Baldock, 2023). Processes-based models (e.g., Roelvink et al., 2009, 2018) have been adapted for coral reef-lined coasts by modifying the typical wave action and/or non-linear shallow water equations and parameterizing the hydrodynamic roughness in wave and friction factors (Van Dongeren et al., 2013; Quataert et al., 2015; Buckley et al., 2018; Lashley et al., 2018; de Ridder et al., 2021). However, although accurate, these models are very computationally expensive (e.g., Quataert et al., 2020) and therefore too slow for EWS (Winter et al., 2020; WMO, 2022b). To capture the accuracy

65   of process-based models in operationally feasible computational time frames, surrogate models, including metamodels (Pearson et al., 2017; Rueda et al., 2019; Liu et al., 2023), machine-learning models (Franklin and Torres-Freyermuth, 2022), and numerical model-informed empirical relations (Beetham and Kench, 2018), have been developed by running process-based models over a limited number of schematic coral reef bathymetries. However, as demonstrated by Scott et al. (2020), the natural variability in coral reef widths, depths, slopes, and rugosities (bathymetric variability) far exceeds the limited schematic

70   bathymetries used in current surrogate models, limiting their accuracy and global applicability in EWS.

To address this need for a fast, accurate EWS that accounts for the natural variability of coral reefs, we developed the Broad-range Estimator of Wave Attack in Reef Environments (BEWARE-2), a computationally efficient meta-process modeling system that estimates runup (wave-driven set-up and swash) based on complex, process-based hydrodynamic model simulations. We developed BEWARE-2 using insights from the development of the BEWARE-1 meta model (Pearson et al.,

75   2017) and real-world coral reef profile clustering techniques of Scott et al. (2020), and trained the model to be suitable for application on a very large range of morphologically diverse, reef-lined coasts. Here we first detail the creation of a training database of representative, morphologically diverse reef profiles and the matching of real-world reef profiles to those representative profiles. Next, we document the application of the process-based hydrodynamic model XBeach Non-Hydrostatic+ (de Ridder et al., 2021) to the representative reef profiles over a broad range of oceanographic forcing conditions to generate

80   hydrodynamic training data. We subsequently describe the application of BEWARE-2 to compute wave runup on a large variety of real-world coral reef profiles, describe the meta-process model validation, and quantify the predictive skill. Lastly, we discuss the meta-process model benefits, limitations, application, and next steps.

2 Methods

The BEWARE-2 meta-process modeling system is based on the non-hydrostatic version (de Ridder et al., 2021) of the open-

85   source, process-based hydrodynamic model XBeach (Roelvink et al., 2009, 2018), henceforth referred to as XBNH, to estimate wave runup (wave-driven setup and swash) on reef-lined coasts. To do so, we developed a training dataset of hydrodynamics and wave runup computed by XBNH for varying hydrodynamic forcing conditions, similar to that of Pearson et al. (2017),

for a set of morphologically diverse reef profiles, based on work by Scott et al. (2020), which is described in the following sections. Here we illustrate the different steps in the development of the meta-process modeling system.

2.1 Model training dataset

2.1.1 Representative reef profiles

A database of 195 representative, cross-reef profiles was created by combining parametric reef profiles from Pearson et al. (2017), real-world reef profiles from Scott et al. (2020), and additional wide reef profiles identified in this study (Figure 1). Coral reef profiles included in the BEWARE-1 model (Pearson et al., 2017) comprise 30 parametric representations of coral reef profile geometries found in literature from 10 sites around the world (Quataert et al., 2015), with reef flat widths ranging from 0–500 m and fore reef slopes from 0.1–0.5. The reef profiles of Scott et al. (2020) and the wide reef profiles identified in this study (defined as profiles that reach a depth of 15 m at distances greater than 1.5 km offshore), were extracted from a dataset of real-world 30,166 coral reef profiles (Storlazzi et al., 2019), covering the coral reef-lined coasts of the United States of America (U.S.), including the States of Hawai'i and Florida; the Territories of Guam, American Samoa, and U.S. Virgin Islands; and the Commonwealths of Puerto Rico and the Northern Mariana Islands. The dataset consists of transects with a 2 m cross-shore resolution spaced at 100 m intervals along the 3,300+ kilometers of coastline. Of these transects, Scott et al. (2020) clustered 20,454 profiles with reef widths less than 1.5 km into 500 cluster groups and representative profiles, using data reduction techniques on morphology and hydrodynamics of the reef profiles. To allow for the application of BEWARE-2 in areas with wide reefs, such as barrier or extremely wide fringing reefs, additional profiles were derived in this study from the remaining 9,712 reef transects with widths greater than 1.5 km. These profiles were clustered based on the submerged morphology in an identical fashion to that of Scott et al. (2020), leading to the identification of 20 representative wide reef profiles.

The 550 reef profiles described in the previous paragraph (i.e., 30 profiles following Pearson et al. (2017), 500 profiles following Scott et al. (2020), and 20 wide reef profiles), henceforth termed the intermediate representative reef profiles (iRRPs), were subsequently reduced to set of 195 representative reef profiles (RRPs) for application in the BEWARE-2 training dataset. In this, 175 representative reef profiles (RRPs) were developed using the 30 iRRPs of Pearson et al. (2017) and 500 iRRPs of Scott et al. (2020), neither of which contain any very wide coral reef profiles (here termed the 530 normal iRRPs). In general, these 530 normal iRRPs have shapes characteristic of atoll and fringing reef profiles. Following the methodology of Scott et al. (2020), the 530 normal iRRPs were reduced to 175 normal RRPs by means of hierarchical clustering based on two sets of features, namely the submerged morphology and nearshore hydrodynamics, that were assigned equal weighting. In line with Scott et al. (2020), the submerged morphology was expressed through both the profile depth and the inverse wave celerity, where the wave celerity (calculated from linear wave theory assuming a peak wave period T_p of 8 s) was included to give greater weight to shallower areas. The nearshore hydrodynamics features included the wave-driven setup, sea-swell and IG swash, and 2%-exceedance runup ($R_{2\%}$), computed using XBNH for four representative wave conditions. Similarly following Scott et al. (2020), each feature within each subset was transformed using a Min-Max linear scaler and equal weighting within
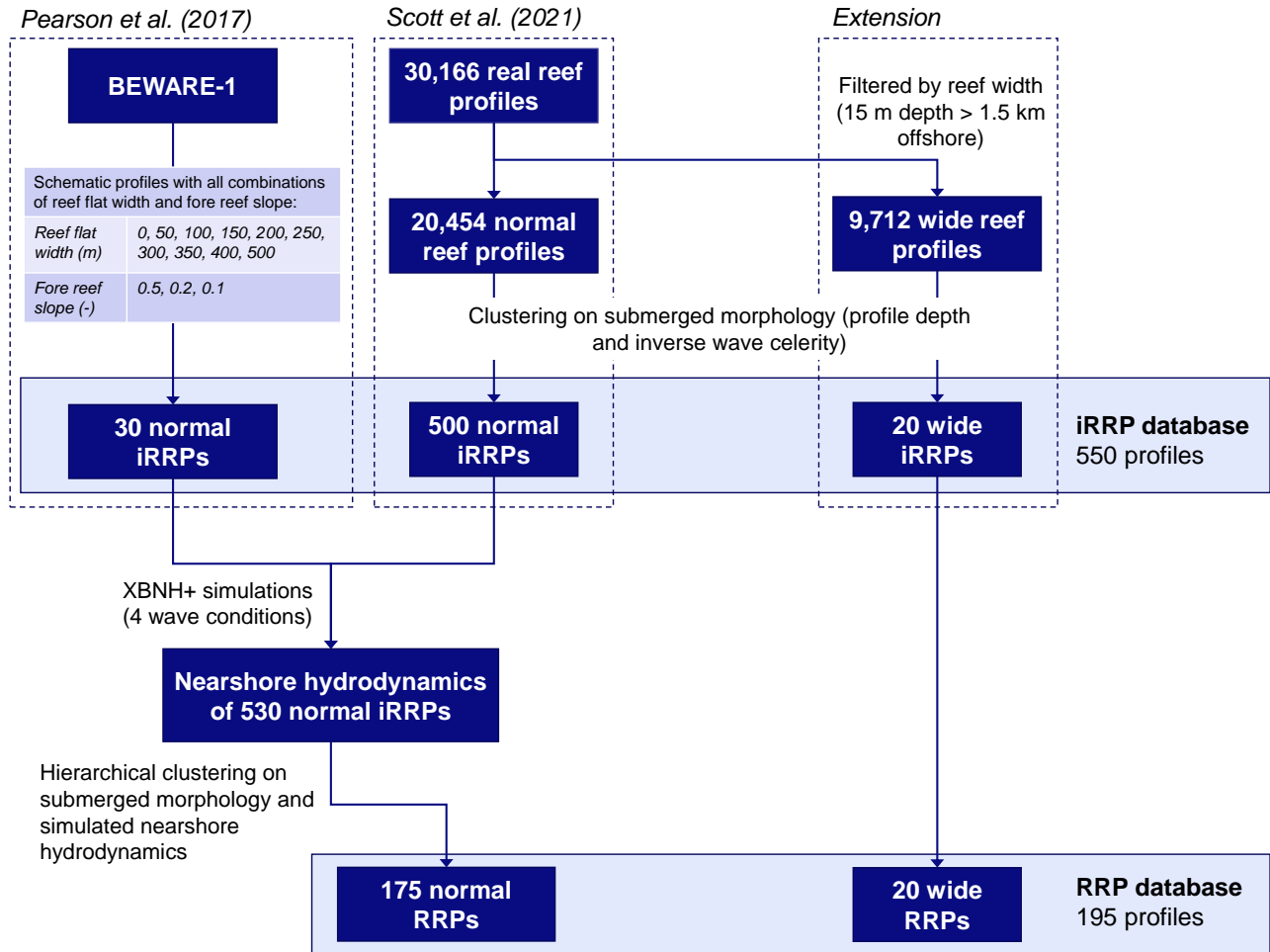
Figure 1. Flow chart outlining datasets and processes to develop both the 550 intermediate (iRRP) and final 195 representative reef profile (RRP) databases encompassing the 30 schematic reef profiles of Pearson et al. (2017), the 20,454 narrow reef profiles of Scott et al. (2020), and the 9,712 wide reef profiles excluded from the Scott et al. (2020) analysis but included here.

the subset was assigned during clustering. During hierarchical clustering, iRRPs were progressively merged based on the smallest intergroup dissimilarity. After merging, an RRP was assigned for each group based on its proximity to the mean $R_{2\%}$. If there were more than one RRP with equal distance to the mean, the RRP that represented the larger number of profiles from the initial round of clustering was chosen. The number of cluster groups was set at 175 profiles based on the intra-cluster similarity of relevant hydrodynamic parameters, which resulted in a relative difference of less than 10% for all four parameters. The 20 wide reef iRRPs were directly mapped to wide reef RRPs and added to the 175 normal RRPs, for a total dataset of 195 RRPs (Figure 2).

125
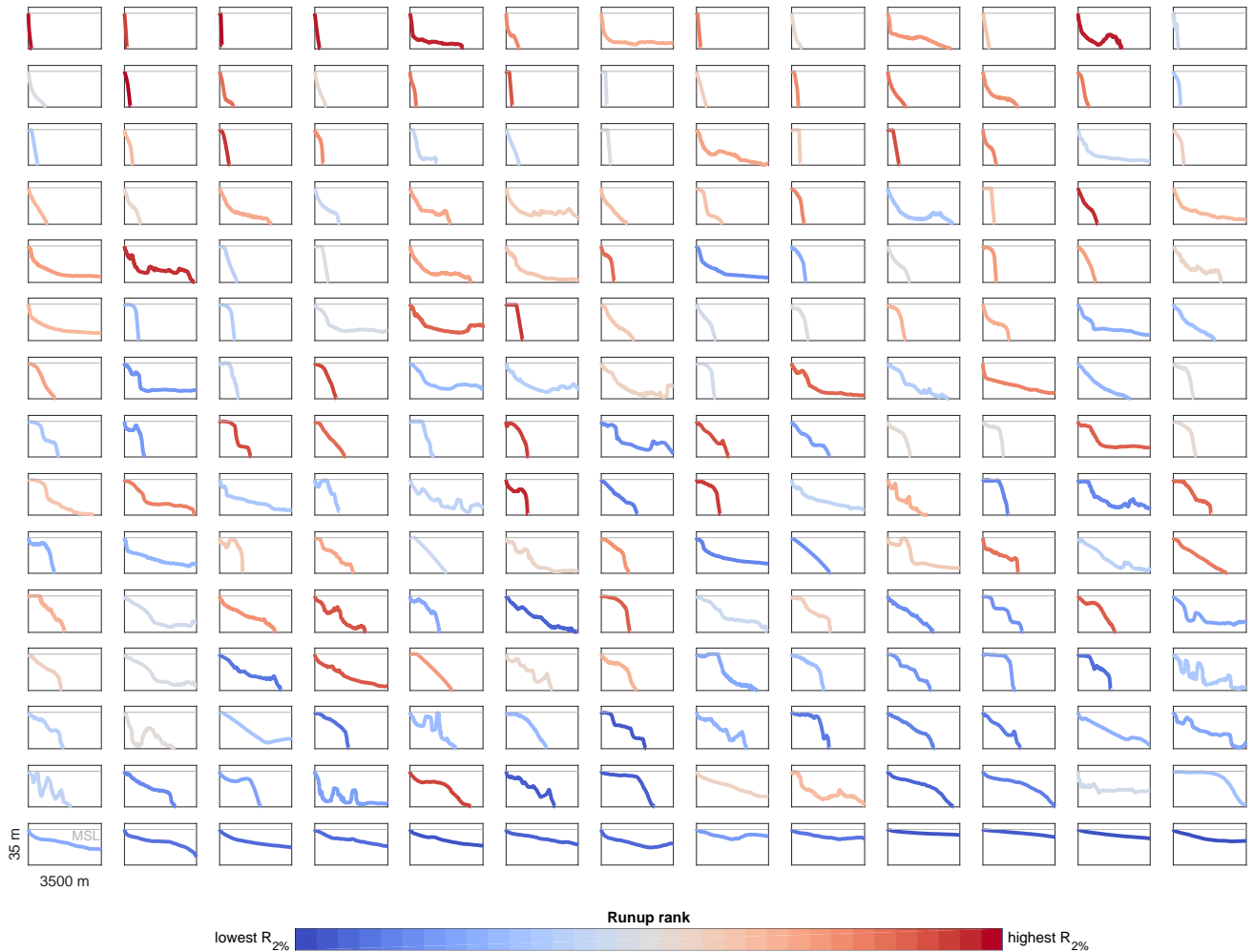
Figure 2. Overview of the morphology of the 195 representative reef profiles (RRPs), ordered from top left to bottom right by cross-shore distance to the 15 m depth contour (W_{reef}, see Section 3.2). The RRPs are color-coded according to the relative ranking of runup simulated by XBNH for a single representative wave condition ($H_{s,0} = 5$ m, $T_p = 12$ s), with blue indicating profiles with relatively lower wave runup and red those with relatively higher wave runup.

2.1.2 XBNH process-based model description and set-up

XBNH is a phase-resolving, non-hydrostatic model for the nearshore and coast. The model solves the non-linear shallow water

130   equations in a reduced 2 vertical-layer system that includes a non-hydrostatic pressure term, allowing application in shallow to intermediate water depth ($kh \lessapprox 4$, where $k = \frac{2\pi}{L}$ is the wave number, h is the water depth, and L is the wave length) with minimal dispersion errors (de Ridder et al., 2021). XBNH and the earlier one-layer non-hydrostatic version of XBeach (Smit

et al., 2010) have previously been shown to reproduce laboratory and field measurements of wave transformation and runup on reef profiles well (e.g., Pearson et al., 2017; Lashley et al., 2018; Klaver et al., 2019; Masselink et al., 2019; Pomeroy and van Rooijen, 2019; Quataert et al., 2020; Masselink et al., 2020; de Ridder et al., 2021; Laigre et al., 2023).

135

XBNH models used for the training and validation of BEWARE-2 were set up in one-dimensional (i.e., cross-shore transect) mode with spatially varying grid resolution and bed roughness. The grid resolution was optimized according to the local water depth and wave period, with a coarser grid being used at greater depths and for longer wave periods (64 points per local wave length; minimum and maximum grid resolution of 0.25 and 5 m, respectively). The reef roughness was parametrized following Storlazzi et al. (2019), with a friction value (c_f) of 0.003 for the sandy beach and deep water. An increased reef friction ($c_f = 0.05$) is implemented at all depths at which $kh \leq 1$ (i.e., depth less than 6.8–91.6 m, depending on the wave period given in Table 1) up to a minimum depth of 0.5 m. The offshore boundary location was established for each individual forcing condition, taking into account depth restrictions of $n = \frac{c_g}{c} < 0.75$, where c_g is the group velocity and c is the wave celerity, to ensure correct infragravity wave boundary condtions, and $kh < 4$ to allow for correct dispersion of the incident-band waves.

145

Additionally, the maximum wave height to depth ratio ($\frac{H_{s,0}}{h}$, where $H_{s,0}$ is the deep water significant wave height) was set to 0.25 to prevent wave breaking at the boundary. Resulting offshore water depths vary between 30 and 58 m. Where necessary, the profiles were extended from the original RRP depth of 30 m to the offshore water depth required for the forcing conditions using a 1/10 artificial slope. To enable computations for the full range of hydrodynamic conditions without runup exceeding the profiles' beach crest, an artificial semi-infinite beach was created extending from 0–30 m MSL with a slope of 1/10. Key model parameters were adopted from Quataert et al. (2020), with model wave breaker parameters *maxbrsteep* and *reformsteep*, which control the onset and cessation of wave breaking in the non-hydrostatic model, set to of 0.6 and 0.3, respectively, and other model parameters set to their default value.

2.1.3   XBNH simulations and output

The XBNH models were developed to simulate wave runup on each RRP for 440 combinations of offshore still water level (SWL; 0–4 m + MSL), $H_{s,0}$ (1–11 m), and T_p (6–22 s), see Table 1 for values applied in this study. To avoid the use of unrealistic wave conditions, $H_{s,0}$–T_p combinations with a deep water wave steepness ($s_0 = \frac{2\pi H_{s,0}}{gT_p^2}$, where g is the gravitational constant) greater than 0.075 were removed. Consequently, no $H_{s,0}$ greater than 4 and 7 m were applied in combination with T_p of 6 and 8 s, respectively. Time series of random realizations of incident-band and wave group-bound IG waves were generated internally by the model (see Roelvink et al., 2009) for each SWL–$H_{s,0}$–T_p forcing combination assuming normally incident offshore waves and a JONSWAP spectral shape (peak enhancement factor $\gamma = 3.3$; Hasselmann et al. 1973) and approximately 24° directional spread ($s = 10$ in cos^{2s} directional spread model). Simulations on all RRPs used the same time series of random incident waves per SWL–$H_{s,0}$–T_p combination to allow for direct comparison of hydrodynamics between RRPs. All simulations were run for a period of 800 T_p (i.e., approximately 800 waves), of which the first 300 T_p period was used as model spin up and model output from the final 500 T_p was used for runup analysis.

165

The XBNH models were set to output the time series of the horizontal and vertical position of the simulated waterline at a temporal resolution of $\frac{T_p}{20}$ (i.e., 0.3–1.1 s). The value of $R_{2\%}$ was derived from the vertical waterline position time series follow-

Forcing parameter	Value
SWL (m + MSL)	0, 1, 2, 3, 4
$H_{s,0}$ (m)	1, 2, 3, 4, 5, 6, 7, 8, 9, 10, 11
T_p (s)	6*, 8*, 10, 12, 14, 16, 18, 20, 22

Table 1. Overview of hydrodynamic forcing conditions used in the training dataset. *Note: wave height combinations for $T_p \leq 8$ s are constrained by maximum deep water wave steepness ($s_0 \leq 0.075$).

ing Stockdon et al. (2006). Output time series for each simulation were split into five time frames of 100 T_p (i.e., approximately 100 waves) to provide five estimates of the empirical $R_{2\%}$ values per simulation. In a limited number of simulations, waterline position time series were split into four or three (6.2 and 2.3% of simulations, respectively) time frames to ensure there were sufficient runup maxima in each period to determine the empirical $R_{2\%}$ value.

In addition to the time series of the simulated waterline, XBNH output time series of water levels, depth-averaged velocity and horizontal discharge were stored at the offshore boundary of the model, eight locations across the reef profile, and 15 positions on the beach face at a temporal resolution of $\frac{T_p}{20}$, which may in the future be used to estimate nearshore wave heights and overtopping rates. These data, although provided in the BEWARE-2 database (https://doi.org/10.5066/XXXXXXXX), are not discussed further in this paper.

2.2 Meta-process model description

Application of BEWARE-2 to estimate wave runup for a given real-world "target" reef profile and real-world "target" oceanic boundary conditions follows a three-step process (Figure 3). These three steps are discussed in the following sections.
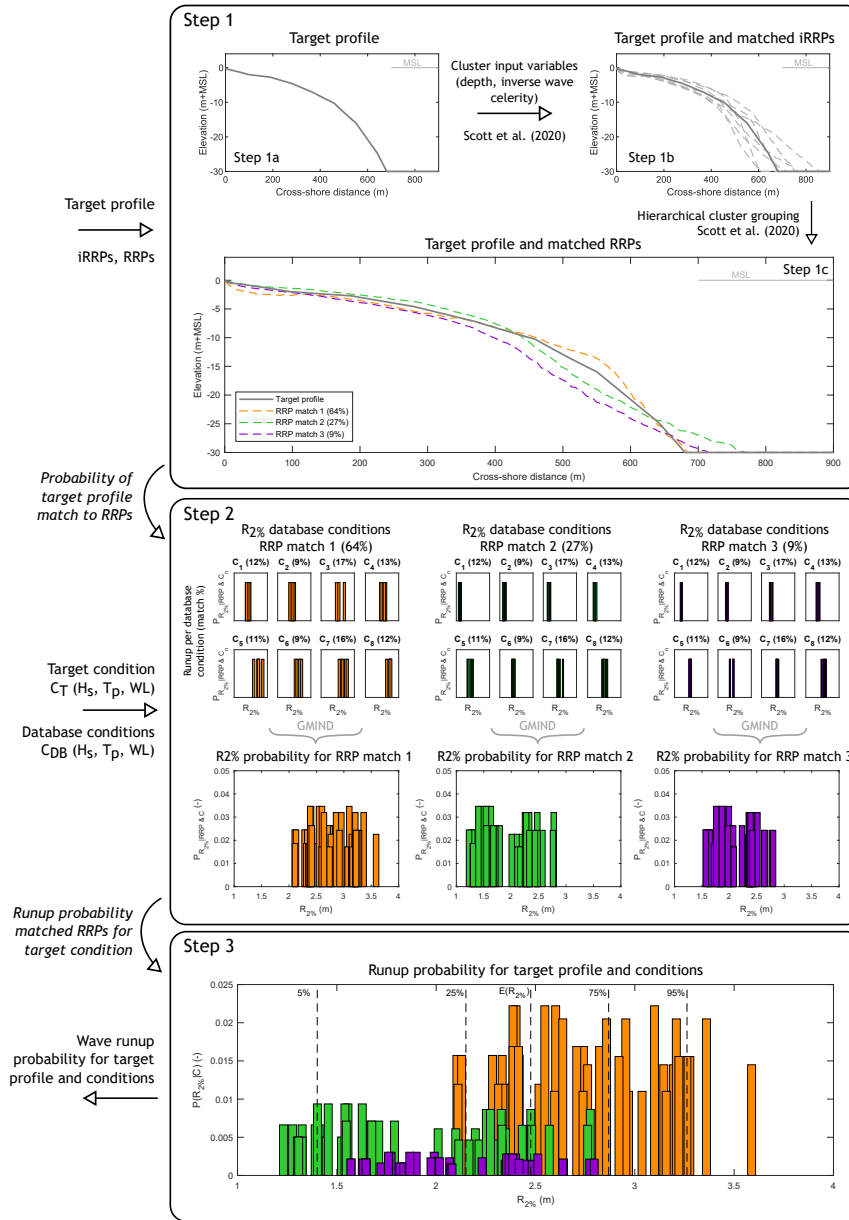
Figure 3. Schematic displaying the steps in application of BEWARE-2 to compute a runup, in this case using three matched representative reef profiles (RRPs) to the real-world, "target," bathymetric profile. Step 1: Matching the target profile to RRPs and their relative match probability. Step 2: For each RRP, extract runup values associated with the oceanographic forcing conditions in the BEWARE-2 database bounding the target oceanographic forcing conditions and their probabilities relative to the target forcing oceanographic conditions using the geometric mean inverse normalised distance (GMIND), Step 3: Combine the database runup probabilities associated with each RRP and their relative weighting to the RRP to compute an expected and/or exceedance probability runup.

2.2.1 Step 1: Matching target bathymetric profile to representative reef profiles (RRPs)

Probabilistic matching of a real-world, "target" bathymetric profile to the representative reef profiles (RRPs) involves three steps (Figure 3, top panel). First, the cluster input variables (i.e., depth and inverse wave celerity) are generated (Step 1a). Second, the target profile is probabilistically matched to the 550 iRRPs (Step 1b). Finally, the result of the matching to the 550 iRRPs is transformed to the 195 RRPs through the hierarchical tree (Step 1c).

The cluster input variables for the probabilistic profile matching in Step 1a are computed following the same procedure for the submerged morphology clustering as Scott et al. (2020), see Section 2.1.1. For both the target profile and the 550 iRRPs, the clustering variables are weighted by 50% for the profile depths and 50% for the inverse wave celerities.

The distance between the target profile and the 550 iRRPs in Step 1b is calculated using the City Block Distance metric (e.g., Melter, 1987). The softmax function (Bridle, 1990) subsequently transforms the vector of real values, in this case the normalized cluster parameter distances, and a stiffness parameter (β_{softmax}) into matching probabilities of the target profile to the iRRPs ($p_{\text{P,iRRP}}$):

$$p_{\text{P,iRRP},i} = \frac{e^{-\beta_{\text{softmax}} d_i}}{\sum_{j=1}^{N_{\text{iRRP}}} e^{-\beta_{\text{softmax}} d_j}} \tag{1}$$

where $p_{\text{P,iRRP},i}$ is the matching probability of the target profile to iRRP i, d_i is the distance between the target profile and iRRP i, d_j is the distance between the target profile and iRRP j, and $N_{\text{iRRP}} = 550$ is the total number of iRRPs.

The stiffness parameter β_{softmax} can be seen as a concentration parameter controlling entropy. Larger values of β_{softmax} result in narrower distributions, corresponding to higher probabilities associated with small absolute distance metrics between the target profile and the iRRPs (and similarly, low probabilities for large absolute distance metrics). The value of β_{softmax} is initially set to 1200, following Scott et al. (2020). A varying β_{softmax} can improve matching outcomes if entropy is too small or large, i.e., many or few iRRPs profiles match the target profile (Bakker et al., 2022). Thus a varying stiffness criteria is established on the distance metric entropy, and ultimately converted to profile matching threshold numbers. Specifically, if the number of iRRPs that a target profile matches to is less than four, β_{softmax} is stepwise relaxed until four iRRPs are matched. Conversely, if the target profile matches more than 10 iRRPs, β_{softmax} is incrementally tightened, with the additional benefit of improving computational efficiency during interpolation.

Finally, in Step 1c, the matched iRRPs are linked to RRPs following the hierarchical clustering tree (i.e., linking 530 iRRPs to 175 RRPs) in the case of regular reef profiles, and in the case of wide reef profiles, the tree branch is a direct iRRP–RRP matching (see Figure 1). Note that due to hierarchical clustering of iRRPs to RRPs, the minimum number of matched RRPs may be less than four. Where multiple matched iRRPs link to the same RRP through hierarchical clustering, the final probability of profile match between the target profile and the RRP ($p_{\text{P,RRP}}$) is computed by summing the match probabilities of all linked iRRPs.

2.2.2 Step 2: Computing runup estimates for matched RRPs based on target oceanic conditions

210 Wave runup estimates for the "target" oceanic forcing condition $C_T(H_{s,0}, T_p, \text{SWL})$ are generated for each matched RRP (Figure 3, center panel). For each matched RRP, all BEWARE-2 $R_{2\%}$ values associated with the oceanic conditions bounding (higher and lower) the target oceanic condition are identified in the BEWARE-2 database, resulting in $2^3 = 8$ bounding oceanic conditions C_{DB} (all combinations of the nearest greater and lesser database values of $H_{s,0}$, T_p and SWL relative to the target oceanic condition). For example, if the target oceanographic conditions are $H_{s,0} = 4.2$ m, $T_p = 13.7$ s, and SWL $= 1.4$ m,

215 $R_{2\%}$ values for all combinations of $H_{s,0} = [4, 5]$ m, $T_p = [12, 14]$ s, and SWL $= [1, 2]$ m conditions would be identified in the BEWARE-2 database. Each BEWARE-2 $R_{2\%}$ value is then assigned a weighting factor proportional to the geometric mean inverse normalised distance (GMIND) between the target oceanographic condition and those in the BEWARE-2 database:

$$\text{GMIND}(n) = \left(\prod_{j=1}^{J} 1 - \left| \frac{X_{j,n} - Y_j}{\Delta X_j} \right| \right)^{\frac{1}{J}} \tag{2}$$

where $n = 1, \ldots, 8$ is the index of the eight (2^J) nearest oceanic conditions in the database, $J = 3$ is the number of oceanic
220 forcing variables (i.e., $H_{s,0}$, T_p and SWL), $X_{j,n}$ is the value of variable j in the database oceanic condition $C_{DB}(n)$, Y_j is the target oceanic condition for variable j, and ΔX_j is the spacing of variable j in the BEWARE-2 oceanic condition dataset.

The probability weighting ($p_{C_{DB}|C_T}(n)$) between the target condition C_T and each of the eight nearest oceanic conditions in the database ($C_{DB}(n)$) is found by normalising GMIND(n) for each C_{DB} condition by the sum of GMIND for all eight C_{DB}:

$$225 \quad p_{p_{C_{DB}|C_T}}(n) = \frac{\text{GMIND}(n)}{\sum_{m=1}^{8} \text{GMIND}(m)} \tag{3}$$

The weighted nearest neighbour-type approach described above to assign probability weights to database conditions is different to the Bayesian-based interpolation applied in the BEWARE-1 meta-model. However, in Section 2.4 we will show that the relatively simple and explainable machine-learning approach applied in BEWARE-2 is easily sufficiently accurate for practical application.

230 2.2.3 Step 3: Compute runup estimate for target profile and target oceanic conditions

To compute the overall expected and/or exceedance probability $R_{2\%}$ for a target profile and target oceanic forcing conditions, the $R_{2\%}$ probabilities of Step 2 ($p_{C_{DB}|C_T}(n)$) are multiplied by the probabilities of profile match of Step 1 ($p_{P,RRP}$; Figure 3, bottom panel). Based on the weighted $R_{2\%}$ values, the expected value and exceedance probability values for $R_{2\%}$ can be established through an empirical cumulative density function.

2.3 Accounting for variations reef roughness and beach slope

The BEWARE-2 training dataset is composed of the results of XBNH simulations on 195 RRPs and under varying conditions of SWL, $H_{s,0}$ and T_p; geometric and hydrodynamic parameters that were found by Pearson et al. (2017) to contribute most to variations in wave runup. However, the training dataset only contains simulations that have constant values for the hydrodynamic roughness of the reef ($c_{f,\mathrm{ref}} = 0.05$) and slope of the subaerial beach ($\beta_{b,\mathrm{ref}} = 0.10$), which were found by Pearson et al. (2017) to contribute least to variations in wave runup. Despite their lesser significance for wave runup on coral reef-lined coasts, inclusion of coral reef roughness and beach slope in BEWARE-2 may be relevant for first-order assessments of the effect of reef health (expressed through c_f) and (seasonal) morphological change of the beach (expressed through β_b) on wave runup. Although it would technically be feasible to include variations in c_f and β_b in the training dataset, this would require an undesirable increase in the number of XBNH simulations and computation time (e.g., a nine-fold increase in computational expense for a minimum of three permutations per parameter, or a 25-fold increase for five permutations per parameter). Therefore, an alternative approach is taken to estimate RRP-specific contributions of reef roughness and beach slope to wave runup.

The methodologies derived to estimate the effect of reef roughness and beach slope variations on wave runup are described in full in Appendix A. In summary, the methodologies utilize a limited dataset of XBNH simulations on 31 reef profiles with varying hydrodynamic parameters and varying values of c_f and β_b (Appendix A1) to calibrate physics-based relations for relative increase or decrease of wave runup using known morphological and hydrodynamic parameters. The resulting relations used to estimate relative changes in wave runup due to variations in reef roughness and beach slope are described in Section 2.3.1 and 2.3.2, respectively. A full description of the derivation and calibration of these relations is given in Appendix A2 and Appendix A3, respectively.

2.3.1 Reef roughness

Increased or decreased wave runup ($R_{2\%}^{m,r}$; Equation 4) relative to the standard BEWARE-2 runup estimate ($R_{2\%}$) due to decreased or increased reef roughness, respectively, is approximated by estimating the relative change in wave height reaching the shore. To do so, a simple wave energy balance model using linear wave theory, the deep water wave conditions, and reef geometry, but excluding bed friction effects, described in Appendix A2, is used to estimate the cross-shore varying near-bed wave orbital (u_{orb}) and wave group (c_g) velocity. This velocity is integrated over the cross-shore extent of the model domain with a hydrodynamic roughness value of $c_f = 0.05$ (L_{c_f}), i.e., the cross-shore extent of the coral reef, to provide a first-order estimate of potential energy loss on the reef due to bed friction (Γ_{reef}; Equation 7). The potential energy loss estimate is subsequently scaled by the difference in roughness of the reef (c_f) relative to the reference reef roughness included in the training dataset ($c_{f,\mathrm{ref}} = 0.05$; Equation 6), $H_{s,0}$, the gravitational constant (g), and a calibration coefficient (α_r) to compute a wave runup modification factor (F_r; Equation 5).

$$R_{2\%}^{m,r} = R_{2\%} F_r \tag{4}$$

$$F_r = \max\left(1 + \alpha_r \frac{\gamma_r}{\sqrt{gH_{s,0}}}\Gamma_{\text{reef}}, 0\right) \qquad (5)$$

$$\gamma_r = \sqrt{\left|\frac{c_f}{c_{f,\text{ref}}} - 1\right|} \qquad (6)$$

$$\Gamma_{\text{reef}} = \sqrt{\int_{L_{c_f}} \frac{u_{\text{orb}}^3(x)}{c_g(x)}dx} \qquad (7)$$

A full description of the derivation of Equations 4–7, and the calibration of α_r is given in Appendix A2. In summary, separate values of α_r were calibrated for reef profiles with relatively low roughness and relatively high roughness, resulting in $\alpha_{r,\text{smooth}} = 1.16$ for a relatively smooth reef ($c_f = 0.01$), and $\alpha_{r,\text{rough}} = -0.65$ for a relatively rough reef ($c_f = 0.10$). Although the application of these calibrated values is intended to illustrate likely upper and lower limits of wave runup for natural reefs in poor or good health, interpolation between the calibrated values for specific intermediate values of c_f likely exceeds the accuracy of the methodology and is therefore not recommended.

2.3.2 Beach slope

In an approach similar to that for variations in reef roughness, wave runup on steeper or milder beach slopes than those included in the BEWARE-2 training dataset ($R_{2\%}^{m,b}$) can be estimated by applying Equation 8. In this, a linear wave runup correction factor (F_b; Equation 9), inspired by the work of Stockdon et al. (2006), is computed using information in the BEWARE-2 training dataset on the hydrodynamic components of wave runup. Here, η_{surf}, η_{swash}, S_{IG}, and S_{inc} are the surf-zone setup, setup inside the swash zone, infragravity-band swash and incident-band swash components of wave runup, respectively, and $\eta_{\text{surf}} + \eta_{\text{swash}} = \eta_{\text{wl}}$ represents the combined time-averaged setup at the shoreline. Following Stockdon et al. (2006), variations in beach slope (β_b) are assumed to affect S_{inc}, but not S_{IG}. Furthermore, it is assumed that the beach slope affects water level set-up at the shoreline (Stockdon et al., 2006), but that this can be separated into a surf-zone component, which is assumed to depend only on the reef and shoreface morphology, and a beach slope-dependent swash-zone component. The contribution of beach slope variations to S_{inc} and η_{swash} is set through the calibration coefficient α_b.

$$R_{2\%}^{m,b} = R_{2\%}F_b \qquad (8)$$

$$F_b = \frac{\overline{\eta_{\text{surf}}} + \alpha_b\overline{\eta_{\text{swash}}} + \frac{\sqrt{S_{\text{IG}}^2 + (\alpha_b S_{\text{inc}})^2}}{2}}{\overline{\eta_{\text{surf}}} + \overline{\eta_{\text{swash}}} + \frac{\sqrt{S_{\text{IG}}^2 + S_{\text{inc}}^2}}{2}} \qquad (9)$$

Although it might be expected that α_b would scale linearly with changes in beach slope, comparison to the calibration data (Appendix A3) shows that linear scaling does not improve the predictive skill of the model. Instead, a heuristic non-linear relation is found between α_b and the change in beach slope (Equation 10):

$$\alpha_b = \left(\frac{\beta_b}{\beta_{b,\text{ref}}}\right)^{\kappa_b} \tag{10}$$

where $\beta_{b,\text{ref}} = 0.10$ is the reference beach slope included in the BEWARE-2 training dataset. The value of $\kappa_b = \frac{1}{e}$ was calibrated by minimizing the RB of the predicted wave runup in the calibration dataset, as described in Appendix A3. As the non-linear nature of Equation 10 is not fully understood, extrapolation for beach slopes outside the range of the calibration simulations (i.e., $\beta_b = 0.05$–0.20) is not recommended.

2.4 Meta-process model validation

2.4.1 Validation dataset

The ability of the BEWARE-2 meta-process model to predict $R_{2\%}$ on morphologically diverse reefs and under varying hydrodynamic forcing conditions is quantified using a validation dataset of 24,000 process-based, XBNH model simulations that are separate from the dataset of simulations used to train the meta-process model. To develop the validation dataset, five normal, and one to two wide, real cross-shore profiles were selected from each of the seven geographic regions (Guam, Saipan-Tinian, American Samoa, Hawai'i, Florida, Puerto Rico, and the US Virgin Islands) included in the dataset of Storlazzi et al. (2019), for a total of 35 normal and 13 wide reef profiles. Normal reef profiles representative of the morphological diversity at every geographic region in the dataset of Storlazzi et al. (2019, i.e., 20,454 profiles in total, see Section 2.1.1) were selected by first statistically determining the the 5, 25, 50, 75, and 95% depth exceedance values at every cross-shore position (i.e., the depth exceeded by a given percentage of the observed profiles at every cross-shore position; Figure 4, dashed lines). Subsequently, the observed, real-world profiles most similar to the cross-shore varying 5, 25, 50, 75, and 95% depth exceedance values (Figure 4, solid lines) were selected for the validation dataset. Wide reef profiles were similarly selected for each geographic region from the dataset of wide coral reef profiles of Storlazzi et al. (2019, i.e., 9,712 profiles in total, see Section 2.1.1). For all geographic regions except American Samoa, the nearest observed profiles to the 25% and 75% depth exceedance of wide profiles were selected for the validation dataset. In American Samoa, the only wide profile included in the database of Storlazzi et al. (2019) was selected. None of the 48 (35 normal and 13 wide reef) validation profiles were identical to the RRPs included in the training dataset.

The XBNH models were set up for all 48 validation profiles using the same model settings and procedure as described in Section 2.1.2. Each validation profile was forced with the same set of 100 combinations of SWL, $H_{s,0}$ and T_p, where values of SWL, $H_{s,0}$ and T_p were randomly sampled between the minimum and maximum values included in the training dataset (Table 1) following independent uniform probability distributions. In similar fashion to the training dataset, no combinations of $H_{s,0}$
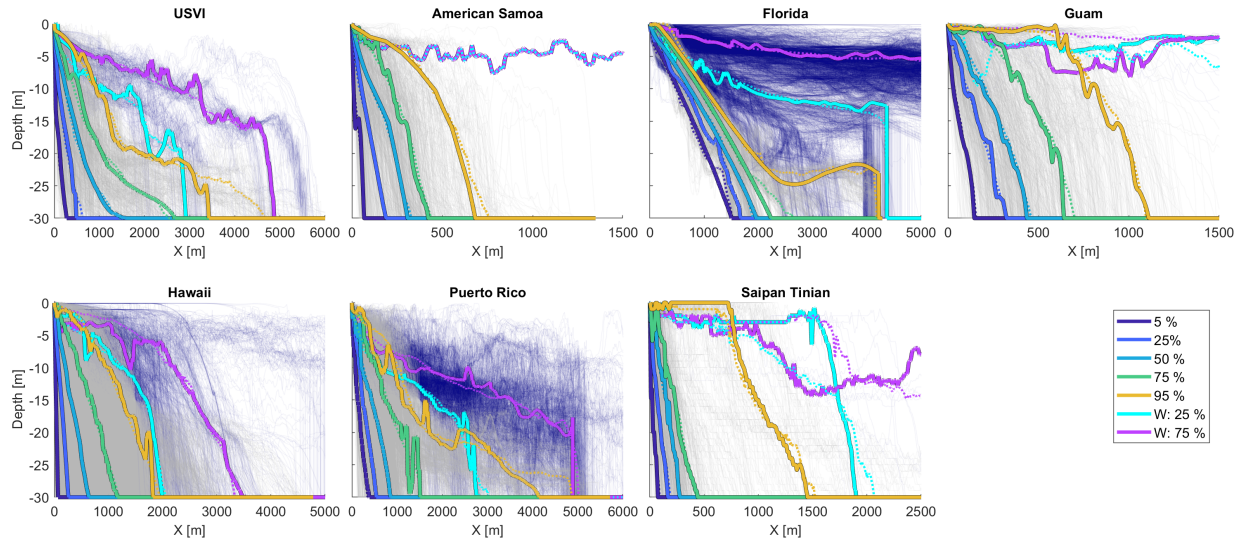
Figure 4. Observed, real-world, normal (gray) and wide (dark blue) cross-shore reef profiles for each of the seven geographic regions included in the dataset of Storlazzi et al. (2019), indicating the natural variability in reef morphologies. Colored dashed lines indicate the cross-shore varying, statistical 5, 25, 50, 75, and 95% depth exceedance values. Colored solid lines indicate the real-world profile most similar to each depth exceedence, which were used for model validation. For the wide reefs, only the 25 and 75% depth exceedance profiles were extracted for model validation.

and T_p with a deep-water wave steepness greater than 0.075 were included in the validation dataset. Wave spectral frequency and directional spread parameters were kept the same as in the training dataset (Section 2.1.3).

Parameter values for the reef roughness and beach slope are initially kept the same as in the training dataset. Thus, the validation dataset contains 4800 simulations (48 profiles, 100 oceanic forcing conditions) with the trained values for reef roughness ($c_{f,\mathrm{ref}} = 0.05$) and beach slope ($\beta_{b,\mathrm{ref}} = 0.10$). However, to validate the $R_{2\%}$ modification relations for reef roughness and beach slope described in Sections 2.3.1 and 2.3.2, additional XBNH simulations were carried out for each combination of validation reef profile and oceanic forcing condition in which either the reef roughness ($c_f = 0.01$, or $c_f = 0.10$), or the beach slope ($\beta_b = 0.05$, or $\beta_b = 0.20$) was increased or decreased relative to $c_{f,\mathrm{ref}}$, or $\beta_{b,\mathrm{ref}}$, respectively. These reef roughness and beach slope variations compose 19,200 simulations (four variations of roughness and slope for all 4800 reef profile – oceanic forcing condition combination).

The combined 24,000 XBNH validation simulations were run for a period of 800 T_p (of which the first 300 T_p was used as spin up), as was the case for the training dataset. $R_{2\%}$ simulated in the XBNH validation models was derived as described in Section 2.1.3. BEWARE-2 $R_{2\%}$ predictions were calculated using the profile matching and $R_{2\%}$ extraction procedures described in Section 2.2. Where relevant, BEWARE-2 $R_{2\%}$ predictions were modified for the reef roughness and beach slope following the procedures described in Section 2.3.

2.4.2 Model skill quantification

The skill of the BEWARE-2 meta-process model in reproducing $R_{2\%}$ simulated by XBNH for the validation dataset was quantified by five measures of accuracy: the root-mean-square error (RMSE; Equation 11), the model bias (Bias, Equation 12), the scatter index, or non-dimensional RMSE (SI; Equation 13), the relative, or non-dimensional bias (RB; Equation 14), and the coefficient of determination (R^2, Equation 15).

$$\text{RMSE} = \sqrt{\overline{(X' - X)^2}} \tag{11}$$

$$\text{Bias} = \overline{(X' - X)} \tag{12}$$

$$\text{SI} = \frac{\text{RMSE}}{\overline{X}} \tag{13}$$

$$\text{RB} = \frac{\text{Bias}}{\overline{X}} \tag{14}$$

$$\text{R}^2 = 1 - \frac{\overline{(X' - X)^2}}{\overline{(X - \overline{X})^2}} \tag{15}$$

In Equations 11–15, X represents the $R_{2\%}$ level simulated by XBNH, X' represents the $R_{2\%}$ level predicted by BEWARE-2, and an overbar represents the arithmetic mean.

3   Results

3.1   Profile matching

The first step in the BEWARE-2 meta-process model is the probabilistic matching of the target profile to the database RRPs (see Figure 3). Here, the validation reef profiles (solid colored lines in Figure 4) were probabilistically matched with between three and 10 RRP profiles (N_{match}; median value 5.5) using the methodology described in Section 2.2 (Figure 5 and Table A1). In the majority of cases (32 out of 48), the target profile matching included one RRP with at least a 50% probability of matching ($p_{\text{P,RRP}} > 0.5$). In six cases (US Virgin Islands W:25%, American Samoa W, Florida 95%, Guam W:25%, Saipan-Tinian 95%, and Saipan-Tinian W:25%) the target profile was matched very strongly ($p_{\text{P,RRP}} > 0.9$) to a single RRP. Three cases (American Samoa 50%, American Samoa 75%, and Puerto Rico 75%) had poor probability of matching ($p_{\text{P,RRP}} < 0.3$) for all matched RRPs, with the poorest probability of matching occurring for the American Samoa 75% profile (maximum match probability of 25%).
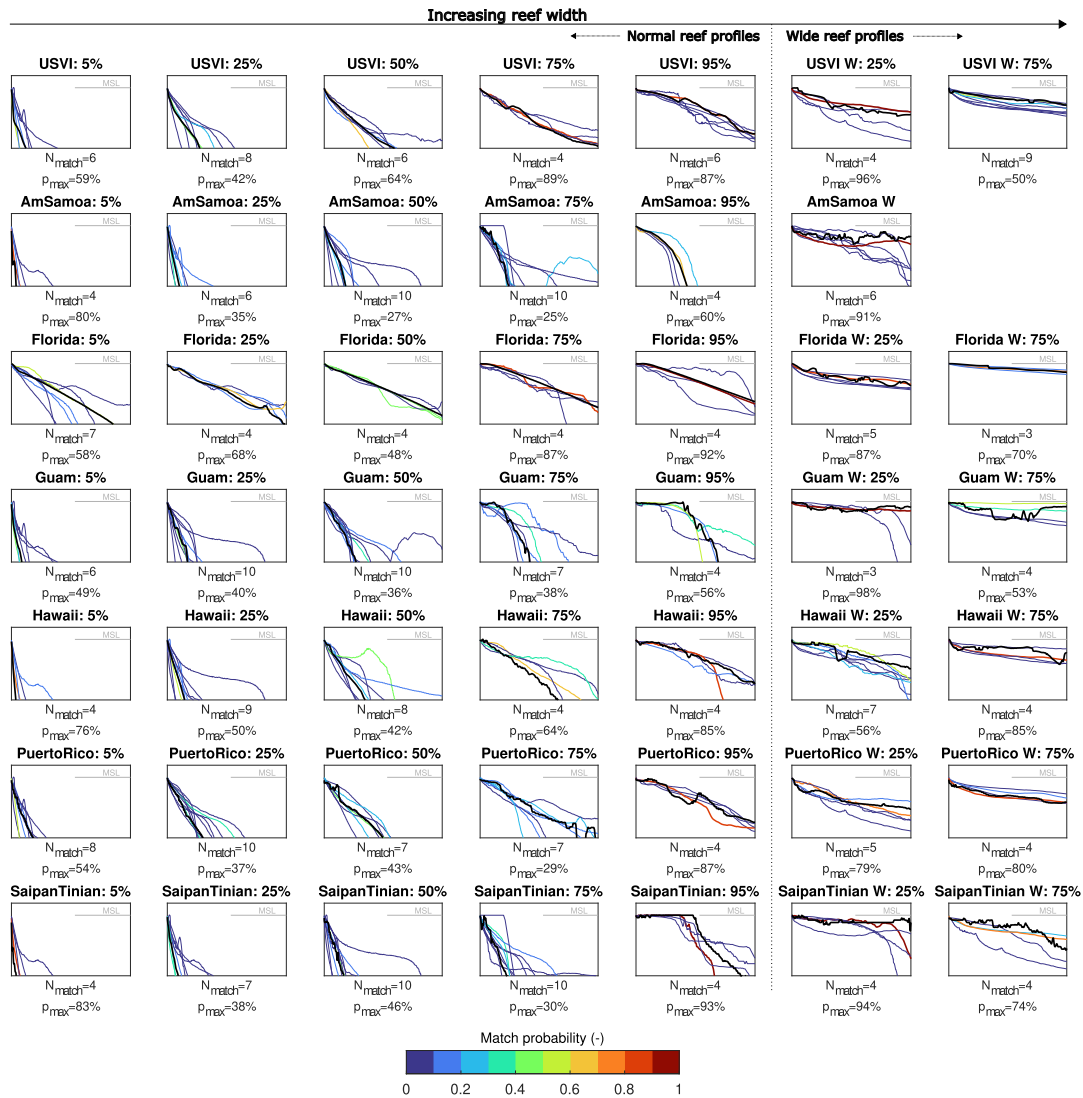
Figure 5. Probabilistic matching of the 48 validation profiles (thick black lines) to RRPs (colored lines). Probability of matching to each RRP is indicated by the color of the RRP. The number of matched RRPs (N_{match}) and maximum matching probability (p_{max}) is given below each panel.

3.2 Runup prediction

Values of $R_{2\%}$ vary substantially between validation profiles (Figure 6), with maximum $R_{2\%}$ on the narrower reef profiles (e.g., 5% profiles of U.S. Virgin Islands, American Samoa, Hawai'i and Saipan-Tinian) approximately 4–5 times greater than on the wide reef profiles. BEWARE-2 $R_{2\%}$ predictions (expected value) compare very well with simulated $R_{2\%}$ results of XBNH almost all 35 normal reef validation profiles, and almost half of the 13 wide reef validation profiles.

370   For the 35 normal reef validation profiles, RMSE and Bias vary between 0.19–0.93 and -0.18–0.75 m, respectively, whereas SI and RB vary between 0.05–0.21 and -0.04–0.18, respectively (see also Table A1). The coefficient of determination is high ($R^2 \geqq 0.80$) for 31 out of 35 validation profiles, and a minimum of $R^2 = 0.64$ (Hawai'i 95%). The two normal validation profiles that matched very strongly to a single RRP have similar accuracy measures to the overall dataset (Florida 95%: SI = 0.15, RB = 0.12; Saipan-Tinian 95%: SI = 0.08, RB = 0.02). Similarly, the three cases that had poor probability of matching

375 do not suffer from a substantial reduction in accuracy (American Samoa 50%: SI = 0.08, RB = 0.05; American Samoa 75%: SI = 0.16, RB = 0.14; Puerto Rico 75%: SI = 0.11, RB = 0.08). Overall, there is no significant correlation (Pearson correlation coefficient 0.01; p-value 0.94) between the accuracy of BEWARE-2 (in this case simplified to only SI, but similar results are found for RB) and the highest probability of matching ($p_{\mathrm{P,RRP}}$) to an RRP. This suggests that the maximum matching probability to RRPs is not a key factor determining model skill, and that the accuracy of the BEWARE-2 meta-process model will remain

380 broadly similar for all normal reef profiles, independent of their morphological similarity to the RRPs.

      For the 13 wide reef validation profiles, RMSE and Bias vary between 0.25–1.17 and -0.81–1.02 m, respectively, whereas SI and RB vary between 0.08–0.43 and -0.16–0.37, respectively. Only 5 of the 13 wide reef validation profiles have a high coefficient of determination ($R^2 \geqq 0.80$). It is therefore apparent that the accuracy of the BEWARE-2 meta-process model is substantially lower on wide reef profiles (e.g., barrier or extremely wide fringing reefs) than on normal reef profiles. Again

385 for the wide reef validation profiles, there is no clear correlation between the accuracy of BEWARE-2 and a high probability matching to RRPs (Pearson correlation coefficient 0.22; p-value 0.47), exemplified by the relatively low accuracy for American Samoa W (one of six cases to match very strongly to one RRP; SI = 0.35, RB = 0.30) and the relatively high accuracy of Hawai'i W:25% (matched to seven RRPs with maximum $p_{\mathrm{P,RRP}} = 0.56$; SI = 0.10, RB = -0.05).
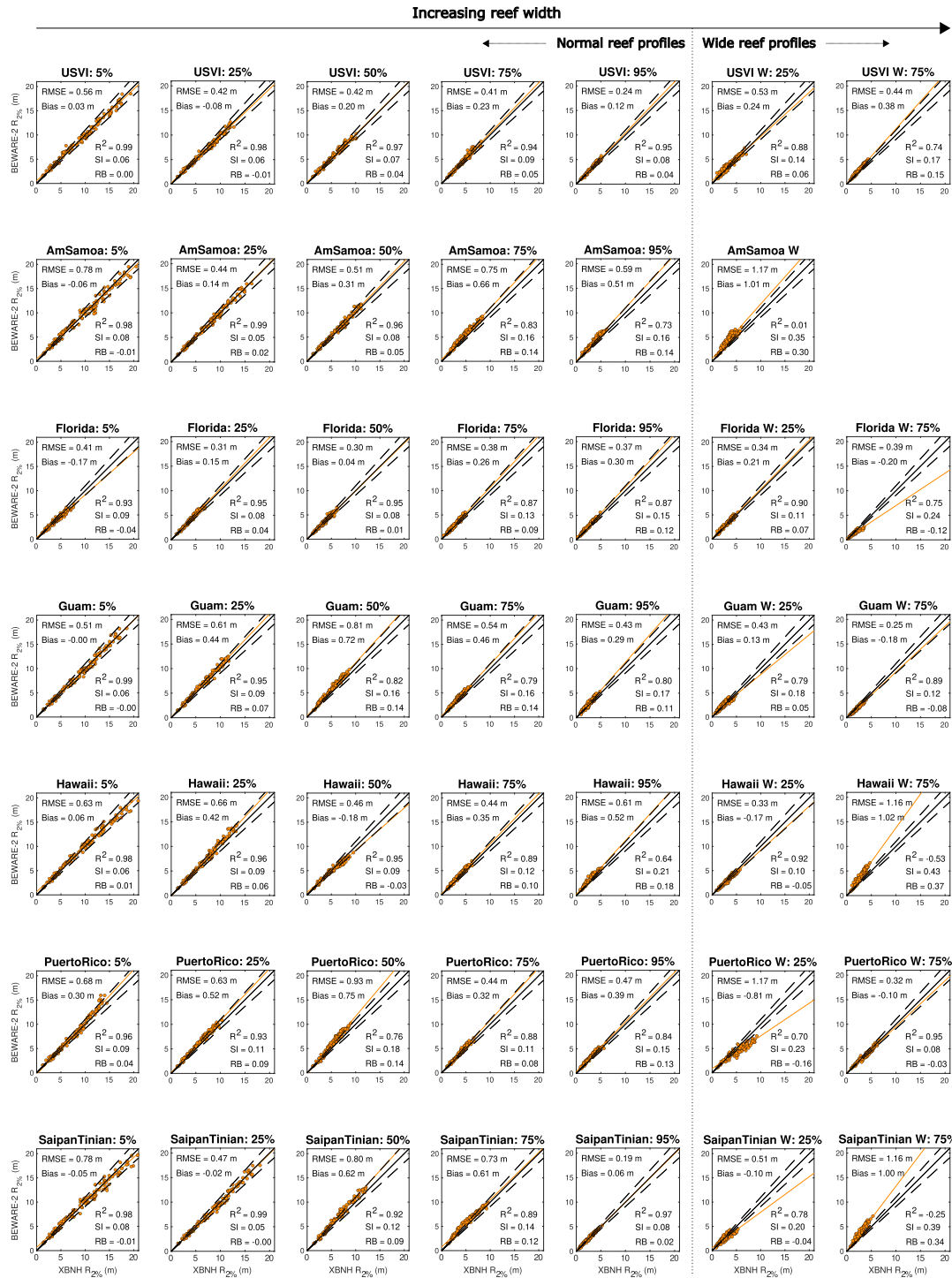
Figure 6. Values of $R_{2\%}$ simulated by XBNH (horizontal axis) and the expected value prediction of BEWARE-2 (vertical axis) for all oceanic forcing conditions and each validation profile. Figures include the 1:1 relation (solid black line), 10% upper and lower deviation from 1:1 (dashed black lines) and the linear regression through the data (solid orange line).

Model skill metrics for the entire validation dataset (Figure 7, left panel) are generally similar to those of the individual

390   validation profiles, with an RMSE and Bias of 0.63 and 0.26 m, respectively, and SI and RB of 0.13 and 0.05, respectively. Model accuracy is generally higher for the 35 normal reef validation profiles (R^2 = 0.98, RMSE = 0.56 m, Bias = 0.26 m, SI = 0.10, RB = 0.05; not shown separately) than for the 13 wide reef profiles (R^2 = 0.72, RMSE = 0.77 m, Bias = 0.25 m, SI = 0.25, RB = 0.08; see also Figure 8, bottom-right panel).

In addition to the expected value of $R_{2\%}$, BEWARE-2 provides the probability of multiple $R_{2\%}$ estimates, based on the

395   probability of profile matching (Section 2.2.1) and the probabilistic interpolation of oceanic forcing conditions included in the training dataset (Section 2.2.2), which can be used to determine empirical $R_{2\%}$ prediction confidence intervals. The 50% confidence interval prediction of $R_{2\%}$ (i.e., 25–75% $R_{2\%}$ prediction interval) is 26% $\pm12\%$ (mean and standard deviation) of the expected value of the prediction (Figure 7, left panel). Whereas 16% of XBNH $R_{2\%}$ values in the validation dataset fall exactly within the narrowest 10% confidence interval (i.e., 45–55% $R_{2\%}$ prediction interval), 67% of all XBNH $R_{2\%}$

400   values fall within the 50% confidence interval prediction, and 92% fall within the 90% confidence interval prediction (Figure 7, right panel). Again, these values are higher when considering only the 35 normal reef validation profiles (18, 75, and 98%, respectively) than when considering the 13 wide reef validation profiles (9, 49, and 75%, respectively). Note that since the BEWARE-2 confidence intervals were determined empirically from information in the training dataset (as well as the profile matching procedure) and applied to the validation dataset, rather than derived directly from the validation data, these results

405   are pertinent and provide valuable information for the application of the BEWARE-2 model.
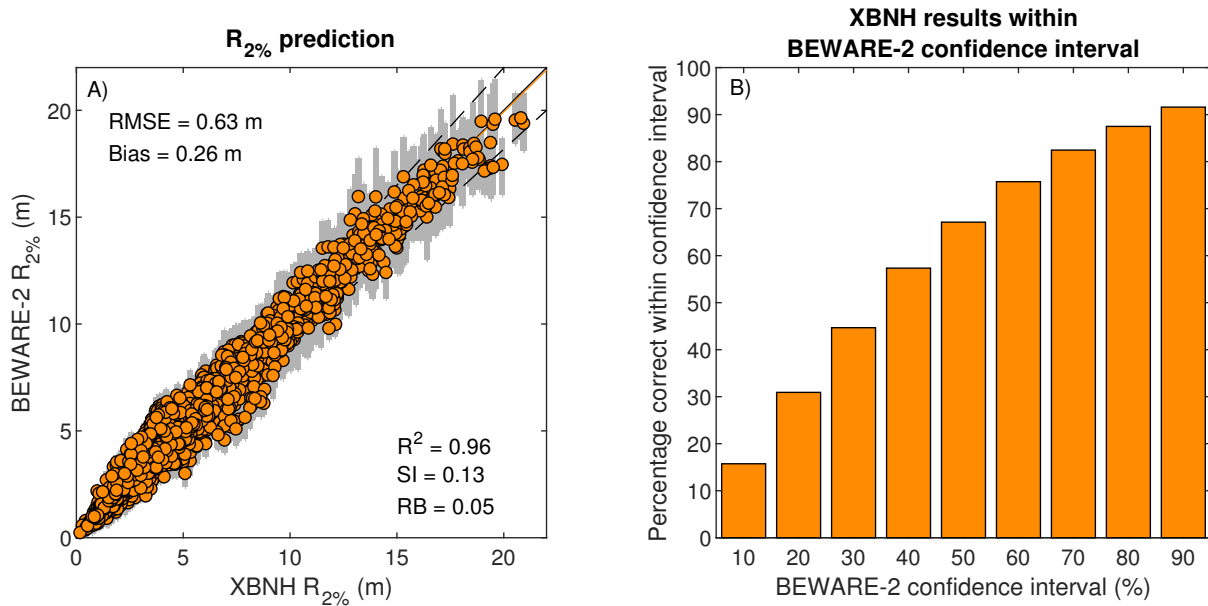
Figure 7. Assessment of $R_{2\%}$ prediction and confidence intervals. A) Comparison of $R_{2\%}$ simulated by XBNH (horizontal axis) and the expected value prediction of BEWARE-2 (vertical axis) for all validation simulations. Included are the BEWARE-2 50% prediction confidence interval (gray vertical bands), the 1:1 relation (solid black line), 10% upper and lower deviation from 1:1 (dashed black lines) and the linear regression through the data (solid orange line). Model skill metrics refer to those of the expected value prediction. B) Percentage of XBNH $R_{2\%}$ values matching BEWARE-2 predictions within BEWARE-2 10–90% confidence intervals.

The model skill for the validation cases differs little for variations in oceanic forcing (Figure 8). The relative measures of model skill R^2, SI, and RB generally improve marginally for increasing H_s (Figure 8, top row) and for decreasing s_0 (Figure 8, second row), whereas RB increases marginally for greater SWL (Figure 8, third row). For all variations in oceanic forcing conditions, the difference in accuracy is insubstantial smaller than the overall accuracy measures (i.e., difference in SI

410 is approximately 10–20% of the overall SI) and will thus likely not affect the practical application of BEWARE-2. Variation in profile steepness, however, expressed through W_{reef} (defined as the cross-shore extent between the shoreline and the 15 m depth contour), again highlights the substantially lower R^2 and higher SI values (i.e., lesser accuracy) for very wide reef profiles, compared to those of narrow to moderately wide (i.e., $W_{\text{reef}} < 1500$ m) reef profiles (Figure 8 bottom row).

The skill metrics of BEWARE-2 are relatively insensitive to the selection of the minimum number of iRRPs the target profile

415 is matched to. In sensitivity simulations using between two and six matched iRRP profiles at minimum, the median skill metrics for all 49 validation profiles changed by less than 8, 11, and 1%, for SI, RB and R^2, respectively. For instance, the median SI value for the 49 validation profiles in the sensitivity simulations ($SI = 0.10$–0.12) is less than 8% change relative to the median SI value for the standard case of minimum four matched iRRPs ($SI = 0.11$).
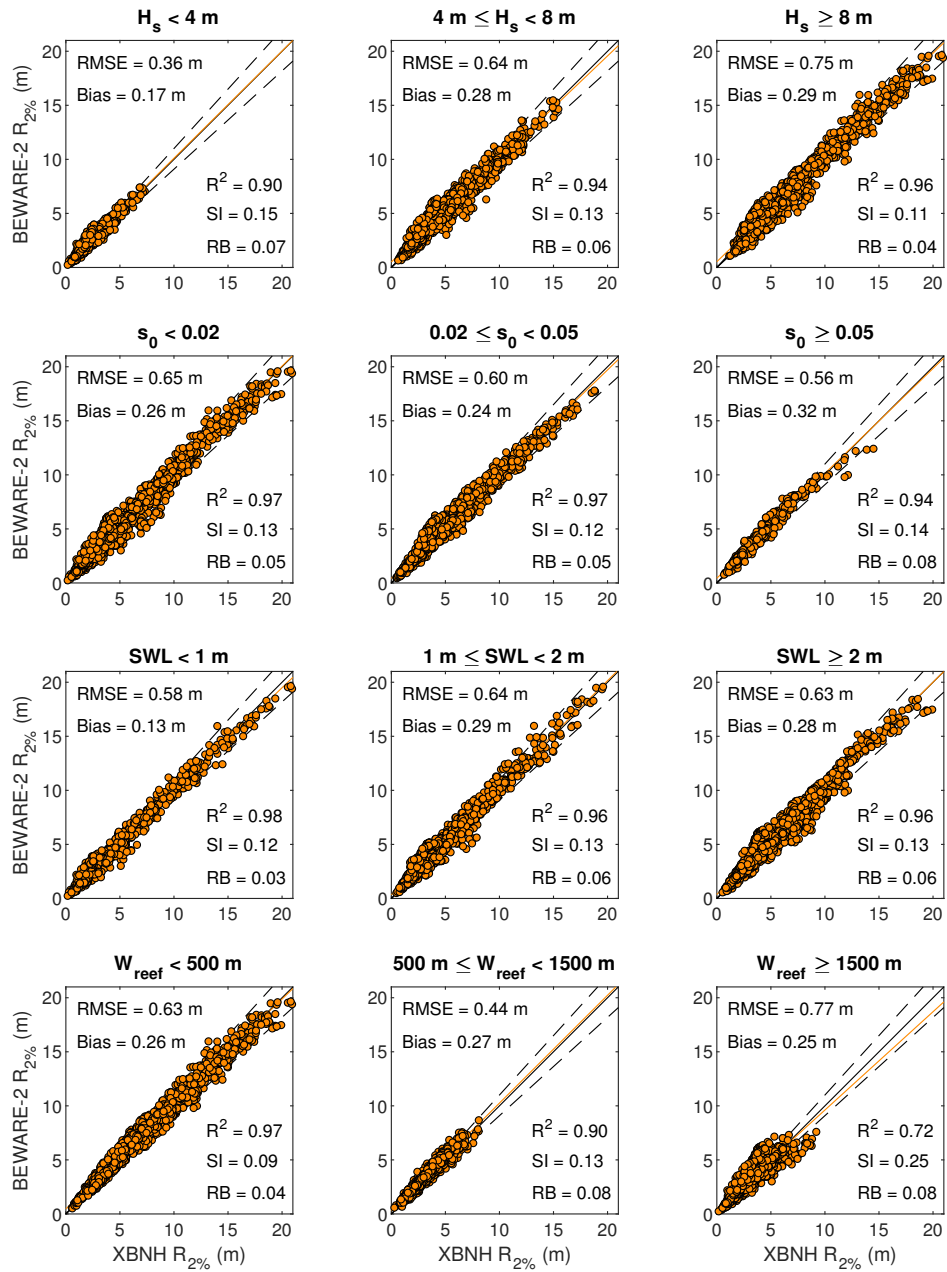
Figure 8. Wave runup simulated by XBNH (horizontal axis) and the expected value prediction of BEWARE-2 (vertical axis) for variations in deep water wave height (top row), deep water wave steepness (second row), still water level (third row) and reef width (bottom row). Figures include the 1:1 relation (solid black line), 10% upper and lower deviation from 1:1 (dashed black lines) and the linear regression through the data (solid orange line).

3.3   Prediction of reef roughness and beach slope effects

420   The wave runup computed by XBNH for simulations with increased or decreased reef roughness and beach slope are compared to BEWARE-2 predictions of wave runup without and with the use of Equations 4 and 8 ("Uncorrected" and "Corrected" columns in Figure 9, respectively). Application of these correction factors substantially increases predictive skill of BEWARE-2 for the validation profiles, with the RB decreasing by a factor of 1.5–6.5 compared to BEWARE-2 predictions without correction factors.
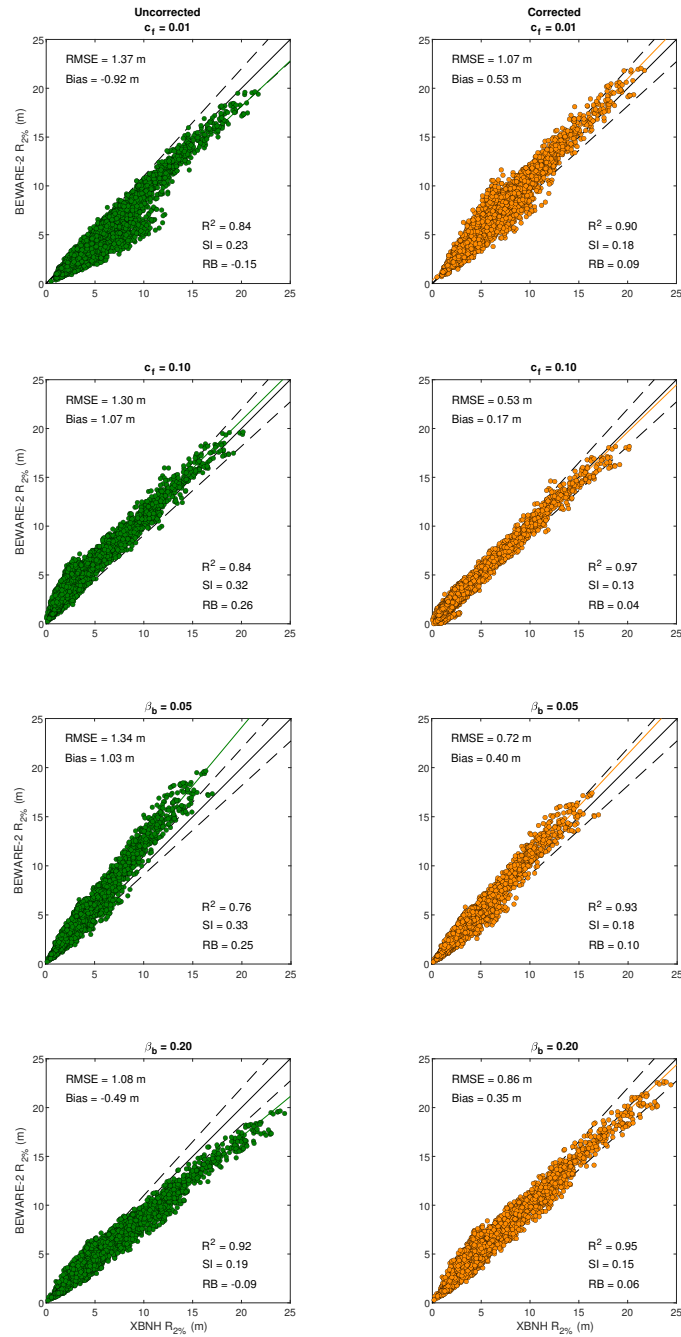
Figure 9. Wave runup simulated by XBNH (horizontal axis) and the expected value prediction of BEWARE-2 (vertical axis) for variations in the hydrodynamic roughness of the reef (c_f; upper two rows) and beach slope (β_b; lower two rows), without (left panels, green) and with (right panels, orange) application of Equations 4 and 8. Included here are the 1:1 relation (solid black line), 10% upper and lower deviation from 1:1 (dashed black lines) and the linear regression through the data (solid green and orange lines).

Application of Equations 4 and 8 improves model bias for most validation subsets of oceanic forcing, reef width, reef roughness, and beach slope (indicated by solid markers with values closer to zero in Figure 10). In particular, parametrizing the effect of reef roughness through Equation 4 most greatly improves model bias for moderate to high energy wave events ($H_s \geq 4$ m), moderate wave steepness ($0.02 \leq s_0 < 0.05$), low water levels (SWL < 1 m), and moderate to wide reef profiles ($W_{\text{reef}} \geq 500$ m). Conversely, parametrizing the effect of beach slope through Equation 8 most greatly improves model bias for low wave steepness ($s_0 < 0.02$), high water levels (SWL ≥ 2 m), and narrow reef profiles ($W_{\text{reef}} < 500$ m).

Equations 4 and 8 do, however, systematically overpredict wave runup (also shown in Figure 9). In certain cases, this over-prediction may (in absolute sense) be greater than the underprediction of the uncorrected BEWARE-2 results. In particular, this is the case for the application of Equation 8 on steep beach profiles ($\beta_b = 0.20$), in combination with high energy wave events ($H_s \geq 8$ m), moderate to steep waves ($s_0 \geq 0.02$), low to moderate water levels (SWL < 2 m), or moderate to wide reef profiles ($W_{\text{reef}} \geq 500$ m). With respect to the application of Equation 4, deterioration in Bias is found only for the validation subset with narrow reef profiles ($W_{\text{reef}} < 500$ m), in combination with decreased reef roughness ($c_f = 0.01$). Note that application of Equations 4 and 8 improves model bias for all oceanic forcing conditions and reef widths in case of increased reef roughness ($c_f = 0.10$) and milder beach slopes ($\beta_b = 0.05$).
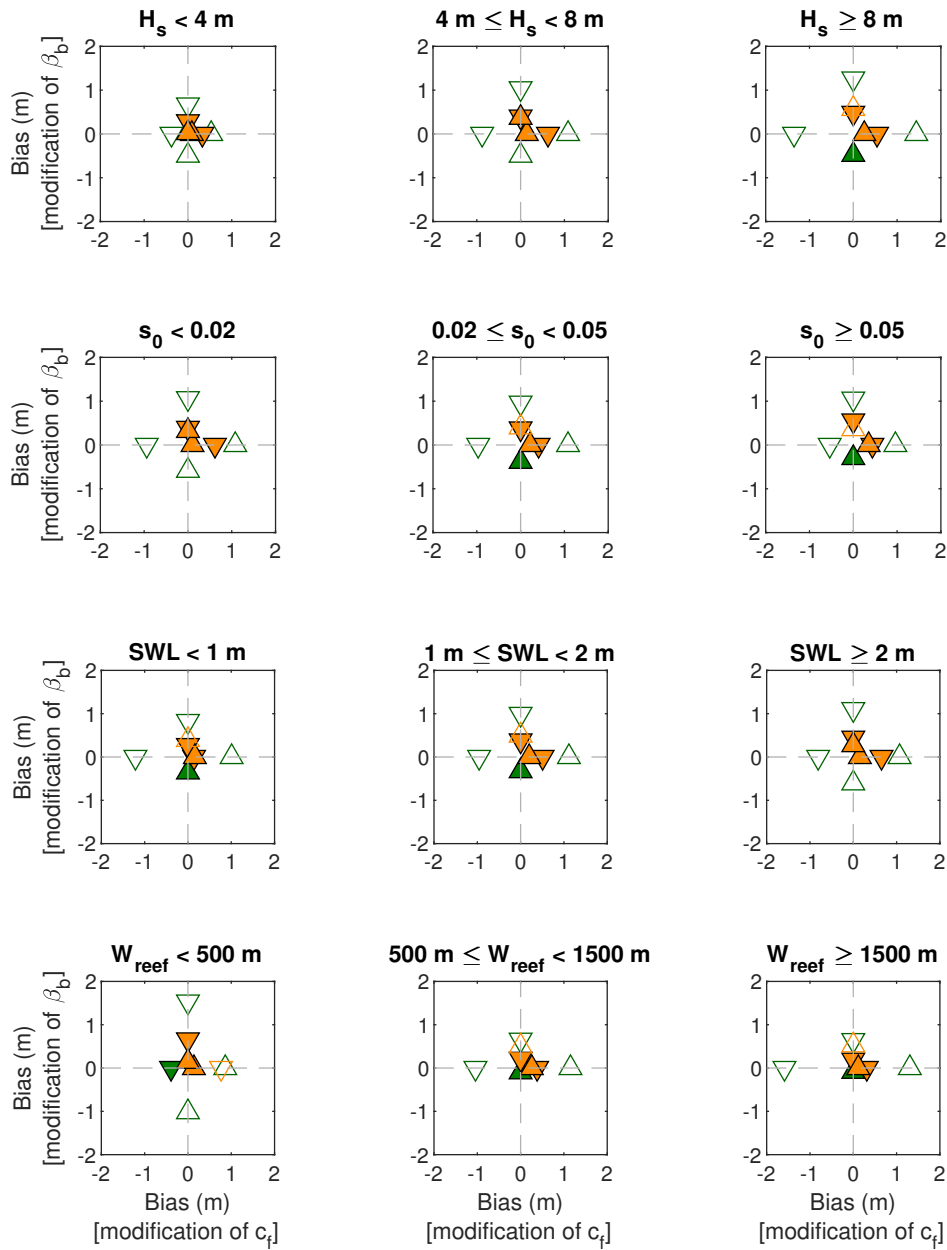
Figure 10. Bias in BEWARE-2 wave runup for simulations with increased ($\triangle$) or decreased ($\triangledown$) reef roughness (c_f; horizontal axis) and beach slope (β_b; vertical axis). Markers are shown for simulations without (green) and with (orange) the use of Equations 4 and 8. Solid green markers indicate that the result without the use of Equations 4 and 8 has the lowest absolute Bias value, whereas solid orange markers indicate lesser Bias with the use of Equations 4 and 8. Results are grouped by deep water wave height (top row), deep water wave steepness (second row), still water level (third row) and reef width (bottom row).

4 Discussion

440 BEWARE-2 was developed to provide a quick, accurate prediction of wave-driven total water levels (setup plus runup) across a wide range of extrinsic oceanographic forcing conditions (SWL, $H_{s,0}$ and T_p) and intrinsic coastal morphological parameters (reef bathymetry, c_f, and β_b). Over a range of 4 m in SWL, 10 m in $H_{s,0}$, and 16 s in T_p across the 48 validation profiles (spanning the range of reef morphologies in seven geographic regions), the meta-process modeling system produced results with an RMSE of 0.63 m and SI of 0.13, with 67% of all $R_{2\%}$ values falling within the 50% confidence interval prediction and

445 92% within the 90% confidence interval prediction of the full, process-based hydrodynamic XBNH model. Incorporating modifications to modeling system to account for variations in c_f and β_b allows systematic errors (RB) in BEWARE-2 predictions to be reduced by a factor of 1.5–6.5. Once having been trained, this relatively accurate solution is provided by the BEWARE-2 meta-process modeling system 4–5 orders of magnitude computationally faster (i.e., $\mathcal{O}(10^{-2})$ s per $R_{2\%}$ prediction) than the full, process-based hydrodynamic XBNH model ($\mathcal{O}(10^2$–$10^3)$ s per $R_{2\%}$ prediction) on a standard desktop computer.

450 ### 4.1 Benefits and limitations of BEWARE-2 model

A key advantage of the BEWARE-2 meta-process modeling system is its ability to estimate uncertainties in the computed runup metrics. The uncertainty range is given by the range of weighted runup results obtained from the XBNH model simulations for the matched RRPs and the nearest (upper and lower) oceanic forcing conditions (SWL, $H_{s,0}$, and T_p). This indication of uncertainty in the computed runup metric (i.e., $R_{2\%}$) would require multiple simulations and post-processing in a deterministic

455 approach, which would come at great computational cost. However, in this implementation the meta-process modeling system will never be equal or better than the underlying process-based model.

The XBNH model is reasonably well validated, as described in the Introduction and Methods sections, but is not perfect. A key limitation of BEWARE-2 is the one-dimensional nature of the underlying XBNH model simulations and thus the meta-process model dataset, which is unlikely to be very accurate in highly two-dimensional situations, such as in the presence of

460 reef channels (e.g., Storlazzi et al., 2022). In addition, BEWARE-2 shows notably lower skill in reproducing XBNH runup values for very wide reef profiles (characteristic of barrier and extremely wide fringing reefs), likely due to the relatively low profile coverage (only 20 RRPs) and large number of possible permutations. Although this may be improved by including a greater number of wide RRPs in the dataset, the real-world accuracy of the underlying XBNH model may likely be lower for very wide reef profiles than other reefs for which it has been validated, as one-dimensional XBNH models are unable to

465 account for wind growth of waves or large-scale topographic refraction (Scott et al., 2020). Further extension of BEWARE-2 for these reef types is therefore currently constrained by the inherent uncertainty in applying XBNH to very wide reef profiles. A final key limitation of BEWARE-2 is the underlying reef profile dataset, which is heavily biased toward data from U.S. (fringing) coral reef-lined coasts (due to consistent LiDAR data availability at the time of BEWARE-2 development) and may lack important other characteristic reef profiles such as barrier and platform reefs. Collection and dissemination of accurate,

470 high resolution bathymetric data at other coral reef-lined coasts around the world would greatly aid application of BEWARE-2, as well as other process-based and meta-models, in global efforts to reduce the impacts of coastal flooding.

4.2 Potential applications of BEWARE-2

The BEWARE-2 meta-process modeling system is fast enough for large-scale application in EWS. As noted by Winter et al. (2020), a coastal flooding EWS would require four main modules: sea levels (including tides and non-tidal residuals), offshore wave conditions, nearshore waves and water levels, and coastal flooding. BEWARE-2 can use the output of global or regional tide models (based on tide station observations and/or satellite altimetry, e.g., TPXO; Egbert and Erofeeva, 2002), global (e.g., HYCOM; Halliwell et al., 1998) or regional general circulation models, or a mix of these models, as SWL input. Offshore wave conditions ($H_{s,0}$ and T_p) for BEWARE-2 can be provided by operational global wave models, such as NOAA GEFS-Wave (utilizing the WaveWatch-III spectral wave model of Tolman, 2009), or region-specific alternatives. Using these oceanographic inputs, BEWARE-2 provides runup, and, in the future, potentially nearshore waves, water levels and overtopping volumes that can be used to assess coastal flooding and thus form the core of an EWS for reef-lined coasts. The primary computational cost of developing an EWS based on BEWARE-2 is pre-processing; developing the BEWARE-2 database and matching of measured reef profiles to the RCP profiles. Once the desired real-world reef profiles have been assigned to the RRPs and the BEWARE-2 database has been linked to the operational water level and wave forecasts, the modeling system can provide a statistical value (e.g., $R_{2\%}$) of runup and measures of its confidence within seconds.

BEWARE-2 can also provide a very rapid first approximation of runup and flooding potential for use in flood risk analyses. In such analyses, the influence of reef health (here expressed in terms of reef roughness following Quataert et al., 2015, and Norris et al., 2023) on runup, and hence flood risk, can be calculated using the BEWARE-2 reef roughness parametrization. Due to the speed of the system, BEWARE-2 can be used simulate 100s of years of runup on a range of profiles with varying reef health to allow climate hindcast and future climate scenario analysis of wave runup. This could help identify coastlines at particular risk of higher and/or more frequent wave runup in the future. Alternatively, BEWARE-2 results can be used to identify relevant nearshore wave and water level conditions in long time series for simulation in other, more computationally expensive, numerical models (e.g., Masselink et al., 2020, 2021).

4.3 Next steps

The BEWARE-2 meta-process modeling system and the underlying process-based hydrodynamic XBNH model ultimately require field validation of both waves and water levels over reefs, and the resulting wave-driven runup on the coast. Such measurements, especially runup, are scarce, but are slowly increasing with the deployment of coastal imaging systems, such as Argus (Holman and Stanley, 2007), in tropical, reef-lined locations. Further testing should also include profiles from non-U.S. reefs that are not included in the dataset used to develop the RRPs, prior to application in other regions.

One of the great aspects of the BEWARE-2 database is its modular nature. The range of oceanographic forcing conditions can be expanded (lower or higher water level and/or wave heights and periods) or refined by additional XBNH simulations. Non-U.S. reef profiles that are morphologically distinct from the current dataset can be included through the addition of new RRPs. Similarly, if one wanted to investigate the role of coral reef restoration in the reef profiles, new RRPs that include the effects of restoration (changes in height and/or bed roughness) could be simulated in XBNH (e.g., Roelvink et al., 2021)

505 and added to the database. Lastly, one could utilize information in the BEWARE-2 dataset to extend prediction variables with output such as overtopping volumes for use in coastal flood modeling studies.

5 Conclusions

A surrogate, meta-process model (BEWARE-2) of the process-based hydrodynamic model XBeach Non-Hydrostatic+ (XBNH; de Ridder et al., 2021) has been developed to estimate wave runup on morphologically diverse reefs. BEWARE-2 builds on

510 work by Pearson et al. (2017) and Scott et al. (2020) to account for a broad range of oceanic forcing conditions (water levels, wave height and period), diverse morphologies of naturally occurring coral reef profiles, and variations in reef roughness and beach slope.

The BEWARE-2 meta-process model accurately reproduces runup (2% exceedance runup level; $R_{2\%}$) simulated by the process-based XBNH model on 48 real-world profiles drawn from seven geographic regions. BEWARE-2 was tested for 100

515 oceanic forcing conditions (combinations of offshore water level, wave height and period), with simulated runup ranging from 0.17 to 20.9 m. BEWARE-2 was shown to have a high overall coefficient of determination ($R^2 = 0.96$) and an overall root-mean square error of 0.63 m (scatter index: 0.13) and bias of 0.26 m (relative bias: 0.05). Model skill differed little for variations in oceanic forcing conditions, but was substantially greater for profiles with reef widths less than 1.5 km ($R^2 = 0.98$, scatter index = 0.10, relative bias = 0.05) than for wider reef profiles ($R^2 = 0.72$, scatter index = 0.25, relative bias = 0.08). Parametric

520 extensions to BEWARE-2 to account for variations in reef roughness and beach slope were shown to reduce systematic errors (relative bias) in BEWARE-2 predictions by a factor of 1.5–6.5 for relatively coarse or smooth reefs, and mild or steep beach slopes.

The simulation of wave runup using BEWARE-2 is 4–5 orders of magnitude faster ($\mathcal{O}(10^{-2})$ s per $R_{2\%}$ prediction) than simulating runup using XBNH ($\mathcal{O}(10^2$–$10^3)$ s per $R_{2\%}$ prediction). In addition, the framework of the BEWARE-2 meta-

525 process model provides a probability distribution of wave runup that can be used to determine the expected value of $R_{2\%}$, alongside confidence bands around this prediction. Key limitations of BEWARE-2 are related to the one-dimensional nature of underlying XBNH model simulations, both for application in highly two-dimensional situations and on very wide reef profiles, as well as the underlying reef profile dataset, which is heavily biased toward data from U.S. coral reef-lined coasts.

The accuracy and speed of the BEWARE-2 meta-process model suggest that it may be a useful tool for early warning systems

530 and current and future coastal flood risk analysis.

Data availability. The BEWARE-2 database presented in this paper is available as a NetCDF (*.nc) file, hosted at the following location: https://doi.org/10.5066/XXXXXXXX [to be added at publication].

Appendix A: Accounting for variations in reef roughness and beach slope

A1   Calibration dataset

535 In a similar approach to the creation of the BEWARE-2 training dataset (Section 2.1.3), a separate and substantially smaller dataset was created for the purpose of developing and calibrating BEWARE-2 wave runup correction factors for smoother and rougher reefs, and steeper and milder beach slopes. To this end, XBNH simulations were carried out on 31 morphologically diverse reef profiles (Figure A1) that were selected through agglomerative hierarchical clustering of the 530 normal reef iRRPs and that represent a subset of the BEWARE-2 RRPs. XBNH simulations were forced using a subset of the hydrodynamic

540 boundary conditions included in the BEWARE-2 training dataset (Table A1). XBNH simulations for all calibration reef profiles and hydraulic boundary conditions were run with the reference reef roughness ($c_{f,\text{ref}} = 0.05$) and beach slope ($\beta_{b,\text{ref}} = 0.10$), as well as for higher ($c_f = 0.10$) or lower ($c_f = 0.01$) reef roughness, or steeper ($\beta_b = 0.20$) or milder ($\beta_b = 0.05$) beach slope (i.e., five c_f–β_b combinations in total). Other XBNH model parameters were set equal to those used for the BEWARE-2 training dataset (Section 2.1.2). XBNH $R_{2\%}$ values for the calibration dataset were calculated as described in Section 2.1.3.

Forcing parameter	Value
SWL (m + MSL)	0, 1, 2, 4
$H_{s,0}$ (m)	1, 3, 5, 7, 9, 11
T_p (s)	8*, 12, 16, 20

Table A1. Overview of hydrodynamic forcing conditions used for the calibration of reef roughness and beach slope effects on wave runup. *Wave height combinations for $T_p = 8$ s are constrained by maximum deep water wave steepness.

A2   Parameterization of reef roughness effect

545

The effect of increased or reduced roughness of the reef relative to $c_{f,\text{ref}}$ on wave runup is not included in the underlying dataset of BEWARE-2. Instead, this effect is parametrized in the model through estimation of the relative increase or decrease in wave height at the toe of the beach due to roughness effects, under the assumption that changes in wave runup will be proportional to changes in the wave height reaching the beach:

550 $$\Delta R_{2\%} \propto \Delta H_{\text{beach toe}} \tag{A1}$$

To estimate the contribution of reef roughness effects on the wave height at the beach toe (defined as the landward edge of the reef located at a depth of 0.5 m, see Section 2.1.2), we assume a stationary wave energy balance on the reef profile:

$$\frac{\partial c_g(x)E(x)}{\partial x} = -D_f(x) \tag{A2}$$
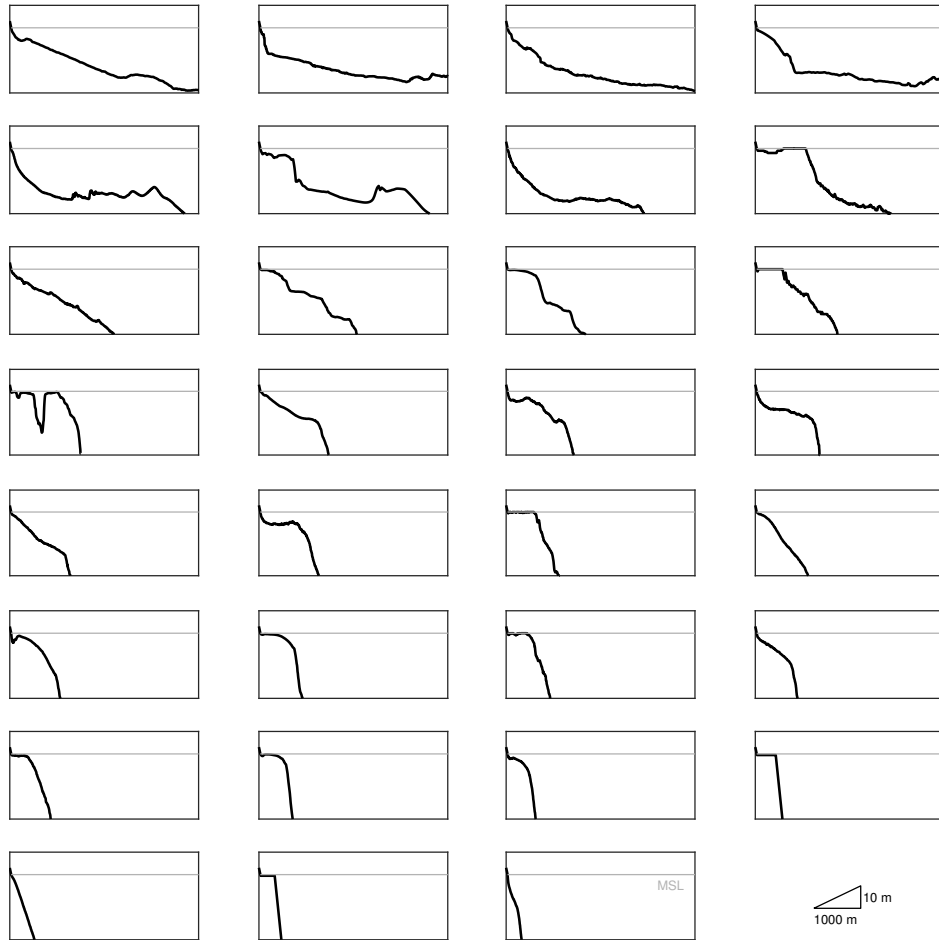
Figure A1. Cross-shore profiles of 31 morphologically diverse RRP reef transects derived by agglomerative hierarchical clustering used to calibrate the parameterization of bed roughness and beach slope effects on wave runup.

in which E is the wave energy, c_g is the wave group velocity, x is the cross-shore coordinate, and $D_f(x) = \frac{2}{3\pi} c_f \rho u_{\mathrm{orb}}^3(x)$ is

555 the wave dissipation term due to reef roughness effects, ρ is the density of water and u_{orb} is the near-bed wave orbital velocity. Note that dissipation due to depth-induced breaking is intentionally not included in Equation A2, but is instead imposed as a boundary condition to the solution in Equation A8.

Through linearisation of the wave group velocity in Equation A2, the integrated wave energy loss across the reef due to reef roughness effects only (ΔE_r) is approximated by:

560 $$\Delta E_r \approx -\int_{L_{c_f}} \frac{D_f(x)}{c_g(x)} dx \tag{A3}$$

in which L_{c_f} is the cross-shore extent of the model domain that has a hydrodynamic roughness value equal to $c_{f,\text{ref}}$, i.e., the cross-shore extent of the coral reef.

Given $H = \sqrt{\frac{8E}{\rho g}}$, the wave height loss across the reef due to reef roughness effects only (ΔH_r) is proportional to:

$$\Delta H_r \propto -\sqrt{\frac{c_f}{g}}\Gamma_{\text{reef}} \tag{A4}$$

565   where Γ_{reef} is the integrated wave dissipation estimate defined in Equation 7.

The assumed proportionality of Equation A1 is combined with the estimated difference in wave height loss across the reef due to varying reef roughness, normalized by the offshore significant wave height ($H_{s,0}$), to derive a proportionality for relative variations in wave runup due to reef roughness effects:

$$\frac{R_{2\%,c_f} - R_{2\%,c_{f,\text{ref}}}}{R_{2\%,c_{f,\text{ref}}}} \propto \frac{\sqrt{\frac{1}{g}}\sqrt{\left|\frac{c_f}{c_{f,\text{ref}}} - 1\right|}\sqrt{\int_{L_{c_f}} \frac{u_{\text{orb}}(x)^3}{c_g(x)}dx}}{H_{s,0}} = \frac{\sqrt{\frac{1}{g}}\gamma_r \Gamma_{\text{reef}}}{H_{s,0}} \tag{A5}$$

570   where $R_{2\%,c_{f,ref}}$ is the wave runup computed for the reference reef roughness value ($c_{f,\text{ref}} = 0.05$) using the underlying XBNH dataset, $R_{2\%,c_f}$ is the estimated wave runup for reef profiles with a higher or lower roughness (c_f) than the reference roughness, and γ_r is the relative reef roughness coefficient defined in Equation 6.

Solving the right hand term in Equation A5 requires an estimate of the local near-bed wave orbital velocity, which is computed as:

575    $$u_{\text{orb}}(x) = \frac{\pi H_{\text{rms}}(x)}{T_p}\frac{1}{\sinh\left(k_p(x)h_0(x)\right)} \tag{A6}$$

where H_{rms} is the root-mean-square wave height, k_p is the wave number based on T_p and h_0 is the local water depth estimated using the cross-shore profile elevation and the offshore still water level (SWL).

The root-mean-square wave height at the offshore boundary of the reef profile ($H_{\text{rms},0}$) is estimated as:

$$H_{\text{rms},0} = \frac{H_{s,0}}{\sqrt{2}} \tag{A7}$$

580   Wave height transformation across the reef profile is estimated using a forward-marching scheme, starting at the offshore boundary of the profile. In this, the computed wave height includes wave shoaling and depth-induced breaking processes, but intentionally neglects dissipation due to hydrodynamic bed roughness:

$$H_{\text{rms}}(x(i)) = \min\left(H_{\text{rms}}(x(i-1))\sqrt{\frac{c_{g,p}(x(i-1))}{c_{g,p}(x(i))}}, \gamma_b h_0(x(i))\right) \tag{A8}$$

where i is the numerical grid cell counter, starting at $i = 1$ at the offshore boundary and increasing in cross-shore direction,

585    $c_{g,p}$ is the wave group velocity estimated using T_p, and $\gamma_b = 0.78$ is the wave breaker index.

Equation A8 allows a first order estimate of wave heights across the reef in the absence of reef roughness effects. Although this method neglects important physical processes (e.g., wave set-up, infragravity wave generation), we find that this first order estimate provides sufficient information with which to derive proportionality constants for Equation A5 and subsequently improve predictions of wave runup on reef profiles with greater and lesser roughness (Section 3.3).

590   Linear proportionality coefficients (α_r) for Equation 5 (and Equation A5) are found separately for relatively smooth ($c_f = 0.01$) and rough ($c_f = 0.10$) reef profiles by computing the left-hand and right-hand terms of Equation A5 for the reef roughness calibration simulations described in A1 and fitting linear least-square error relations to the smooth and rough reef datasets (Figure A2). In this manner, we find proportionality coefficients $\alpha_{r,\text{smooth}} = 1.16$ for relatively smooth reefs and $\alpha_{r,\text{rough}} = -0.65$ for relatively rough reefs, with considerable scatter around the linear fit that is likely due to the extensive simplification

595   of the true hydrodynamics on reef profiles.
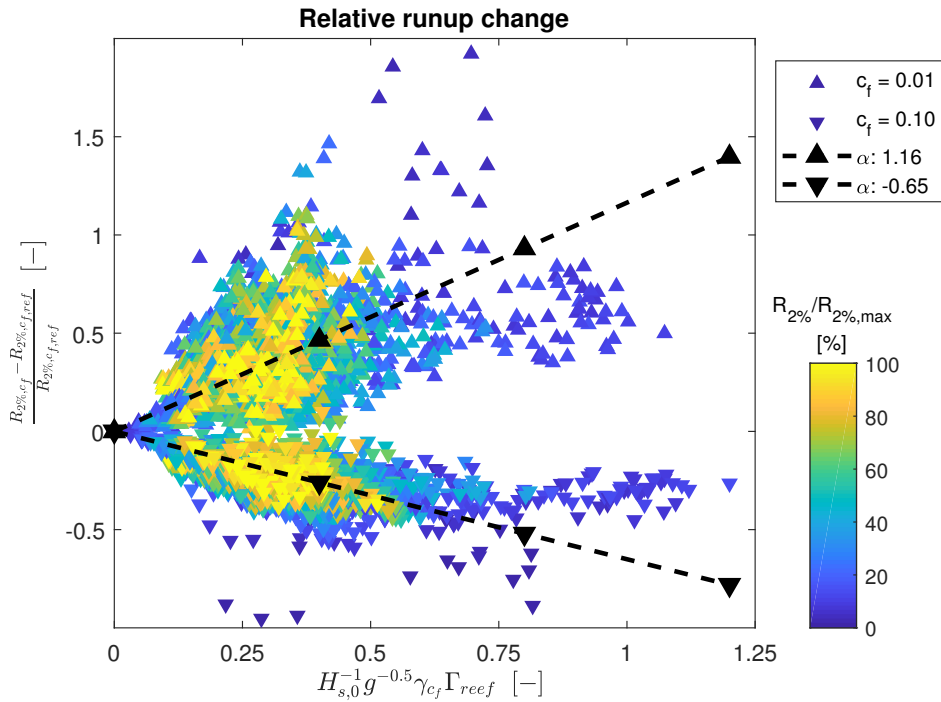
Figure A2. Variation in relative wave runup as a function of the right-hand term of Equation A5. Linear proportionality constants α_r found for reef profiles with lower ($c_f = 0.01$; ▲) and higher ($c_f = 0.10$; ▼) reef roughness are shown as dashed lines. Computed relative runup values are coloured by the computed wave runup relative to the maximum runup in the calibration dataset.

Despite the high degree of simplification present in this methodology, application of the calibrated α_r coefficients to the conditions included in the calibration dataset (A1) greatly improves skill metrics of wave runup (Figure A3). In particular,

application of the calibrated coefficients greatly reduces the bias of the runup predictions (i.e., improvement of RB from -0.25 to 0.00 for smoother reefs, and from 0.30 to 0.02 for rougher reefs), as would be expected from the linear fit methodology. Importantly, as shown in Section 3.3, application of the calibrated α_r coefficients to the validation dataset also substantially reduces model bias and improves the wave runup skill metrics of BEWARE-2.

The two derived values of α_r appear to scale approximately proportionally with the square root of the change in the reef roughness coefficient ($\alpha_{r,\mathrm{smooth}} \approx 0.5\sqrt{\frac{0.05}{0.01}}$; $\alpha_{r,\mathrm{rough}} \approx -0.5\sqrt{\frac{0.10}{0.05}}$), with a change in sign for rougher reefs relative to the reference reef roughness. However, the use of inter- or extrapolated values of α_r for reefs with other representative roughness values is not recommended without further investigation of this relation. Instead, wave runup values computed in BEWARE-2 using $\alpha_{r,\mathrm{smooth}}$ and $\alpha_{r,\mathrm{rough}}$ can be used to illustrate likely upper and lower bounds of wave runup for natural reefs in poor or good health.

A3   Parameterization of beach slope variation effect

Similarly to reef roughness variations, the effect of steeper or milder beach slopes relative to $\beta_{b,\mathrm{ref}}$ on wave runup is not included in the underlying dataset of BEWARE-2. Instead, this effect is parametrized in the model through estimation of the contribution of the beach slope to the incident-band swash and swash-zone setup.

Following Stockdon et al. (2006), we can describe the components of wave runup as:

$$R_{2\%} = c_R \left(\overline{\eta_{\mathrm{wl}}} + \frac{\sqrt{S_{\mathrm{IG}}^2 + S_{\mathrm{inc}}^2}}{2} \right) \tag{A9}$$

where $\overline{\eta_{\mathrm{wl}}}$ is the time-averaged vertical position of the waterline observed at the shore, S_{IG} and S_{inc} are the infragravity and incident-band swash, respectively, and c_R is a regression coefficient found to have a value of 1.1 in the data of Stockdon et al. (2006).

Following Stockdon et al. (2006), we assume that variation in beach slope (in this case $\beta_b = 0.05\text{–}0.20$) will not affect S_{IG}. Furthermore, we assume that the contribution of the surf-zone setup ($\overline{\eta_{\mathrm{surf}}}$) to the setup observed at the shoreline ($\overline{\eta_{\mathrm{wl}}}$) is independent of the beach slope (but instead dependent upon the shoreface and reef profile) and therefore already correct in the underlying training dataset for BEWARE-2. It remains, however, that a beach slope correction factor (α_b) is likely required for the incident-band swash (S_{inc}) and setup occurring within the swash zone ($\overline{\eta_{\mathrm{swash}}} = \overline{\eta_{\mathrm{wl}}} - \overline{\eta_{\mathrm{surf}}}$) to improve wave runup predictions in BEWARE-2 for beach slopes different to $\beta_{b,\mathrm{ref}}$.

To determine the value of α_b we first empirically determine the values of $R_{2\%}$, $\overline{\eta_{\mathrm{wl}}}$, S_{IG}, and S_{inc} from the time series of the waterline elevation (i.e., time-varying swash signal) output by XBNH in all calibration simulations with the reference beach slope ($\beta_{b,\mathrm{ref}} = 0.10$). In this, we compute $R_{2\%}$ as the empirical 2%-exceedance height of swash peaks above still water level, and S_{IG} and S_{inc} from the variance density spectrum of the simulated waterline elevation time series (see e.g., Stockdon et al. 2006; de Beer et al. 2021) using frequency integration limits of $\frac{1}{20}f_p \leq f < \frac{1}{2}f_p$ for the computation of S_{IG} and $\frac{1}{2}f_p \leq f < 3f_p$ for the computation of S_{inc}, where f is frequency and $f_p = \frac{1}{T_p}$ is the offshore wave spectral peak frequency. We derive $\overline{\eta_{\mathrm{surf}}}$ from the mean water level at the nearest XBNH model output point to the toe of the beach, which is located at MSL - 0.5 m and
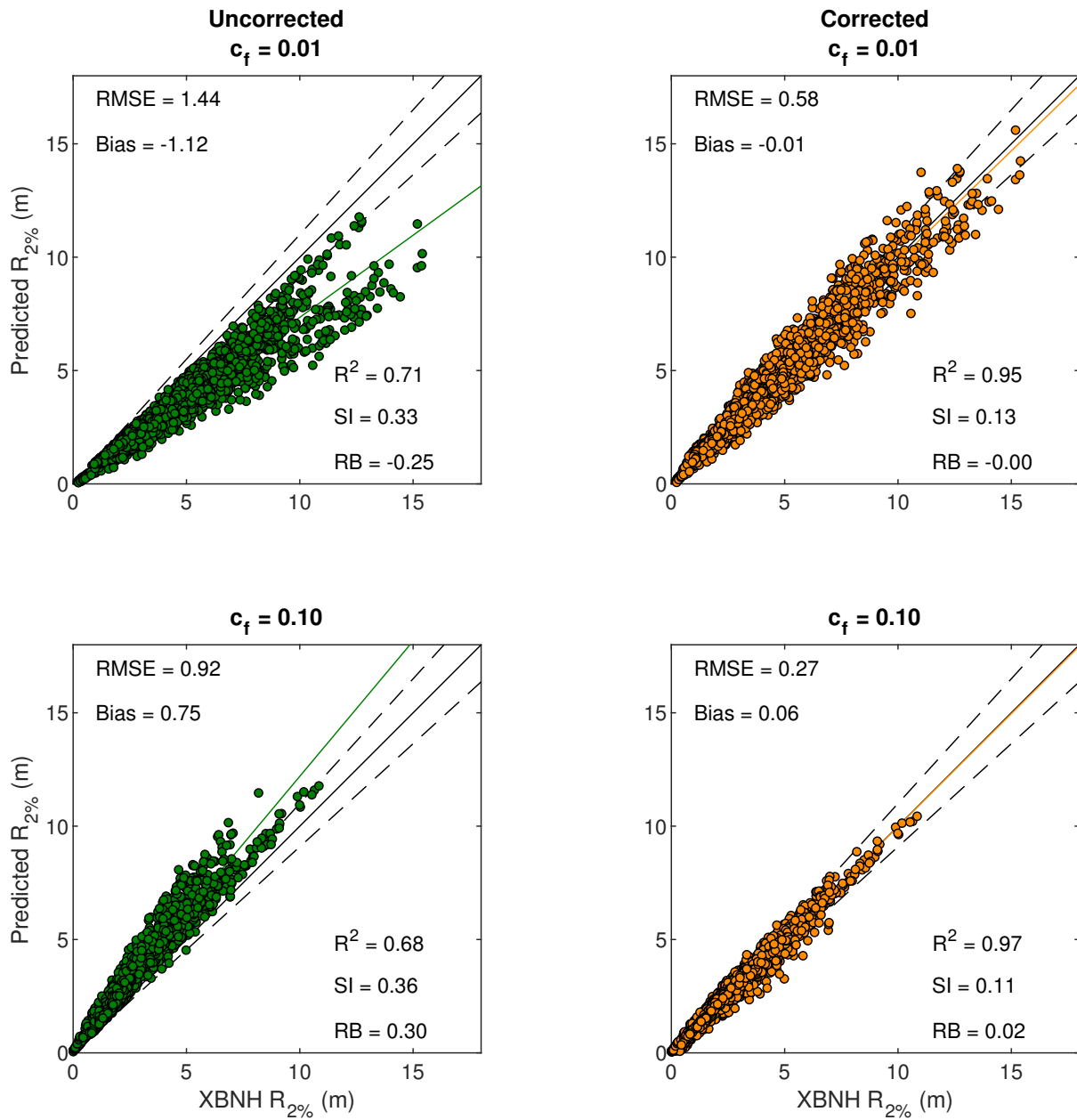
Figure A3. Wave runup predicted by BEWARE-2, without (left panels) and with (right panels) use of α_r, relative to simulated by XBNH for smoother ($c_f = 0.01$; top panels) and rougher ($c_f = 0.10$; bottom panels) reefs than the reference reef roughness ($c_{f,\text{ref}} = 0.05$) in the calibration dataset. Figures include the 1:1 relation (solid black line), 10% upper and lower deviation from 1:1 (dashed black lines) and the linear regression through the data (solid green and orange lines).

$\overline{\eta_\text{swash}}$ from the time-averaged waterline elevation. We subsequently calculate the value of c_R separately for every simulation as $c_R = \frac{R_{2\%}}{\overline{\eta_\text{wl}} + \frac{\sqrt{S_\text{IG}^2 + S_\text{inc}^2}}{2}}$, thereby ensuring that application of Equation A9 with simulation-specific values of c_R provides an exact representation of the waterline time series-derived $R_{2\%}$-value. The values of c_R computed in this manner range between 0.92 and 2.04 (median value 1.16).

Given the computed values of c_R, $\overline{\eta_\text{surf}}$, $\overline{\eta_\text{swash}}$, S_IG and S_inc for all calibration simulations with the reference beach slope $\beta_{b,\text{ref}}$, we can estimate the wave runup for other beach slopes ($R_{2\%}^{m,b}$) through inclusion of α_b in Equation A9 as follows:

$$R_{2\%}^{m,b} = c_R \left(\overline{\eta_\text{surf}} + \alpha_b \overline{\eta_\text{swash}} + \frac{\sqrt{S_\text{IG}^2 + (\alpha_b S_\text{inc})^2}}{2} \right) \tag{A10}$$

To test the validity of Equation A10, values of $R_{2\%}^{m,b}$ are compared to runup values derived empirically from XBNH simulations for the same RRPs and forcing conditions, but with beach slope set at $\beta_b = 0.05$ and $\beta_b = 0.20$ (see Section A1).

As Stockdon et al. (2006) found both $\overline{\eta_\text{wl}}$ and S_inc to be proportional to β_b, the required beach slope correction factor α_b would be expected to be proportional to the change in beach slope relative to the reference beach slope (i.e., $\alpha_b = \frac{\beta_b}{\beta_{b,\text{ref}}}$). However, we find that if a linear relation between β_b and α_b is used, Equation A10 greatly overestimates the effect of the beach slope on wave runup relative to that simulated by XBNH, showing underestimation of wave runup relative to XBNH for milder beach slopes (Figure A4, top right panel) and overestimation for steeper beach slopes (Figure A4, bottom right panel). In quantitative sense, application of Equation A10 and a linear relation between β_b and α_b even reduces the predictive skill of the model for steep beach slopes ($\beta_b = 0.20$) relative to applying no beach slope correction at all (Figure A4, bottom panels).

Substantial improvement in model predictive skill is found, however, if a non-linear relation is assumed between β_b and α_b in the form of $\alpha_b = (\frac{\beta_b}{\beta_{b,\text{ref}}})^{\kappa_b}$. Through minimization of the combined relative bias (RB) of the runup prediction for both milder and steeper beach slopes, optimal values of κ_b were found in the range 0.35–0.38 (difference in combined RB across range less than 0.5 percentage points), with a value $\kappa_b = \frac{1}{e} \approx 0.37$ selected for application in the model (Equation 10).

Application of Equation 8 using $\kappa_b = \frac{1}{e}$ substantially improves the skill of BEWARE-2 in reproducing XBNH wave runup on milder and steeper beaches in the calibration dataset, see Figure A5. The non-linear nature of Equation 10 is, however, not fully understood and extrapolation for beach slopes outside the range of the calibration simulations (i.e., $\beta_b = 0.05$–0.20) is therefore not recommended.
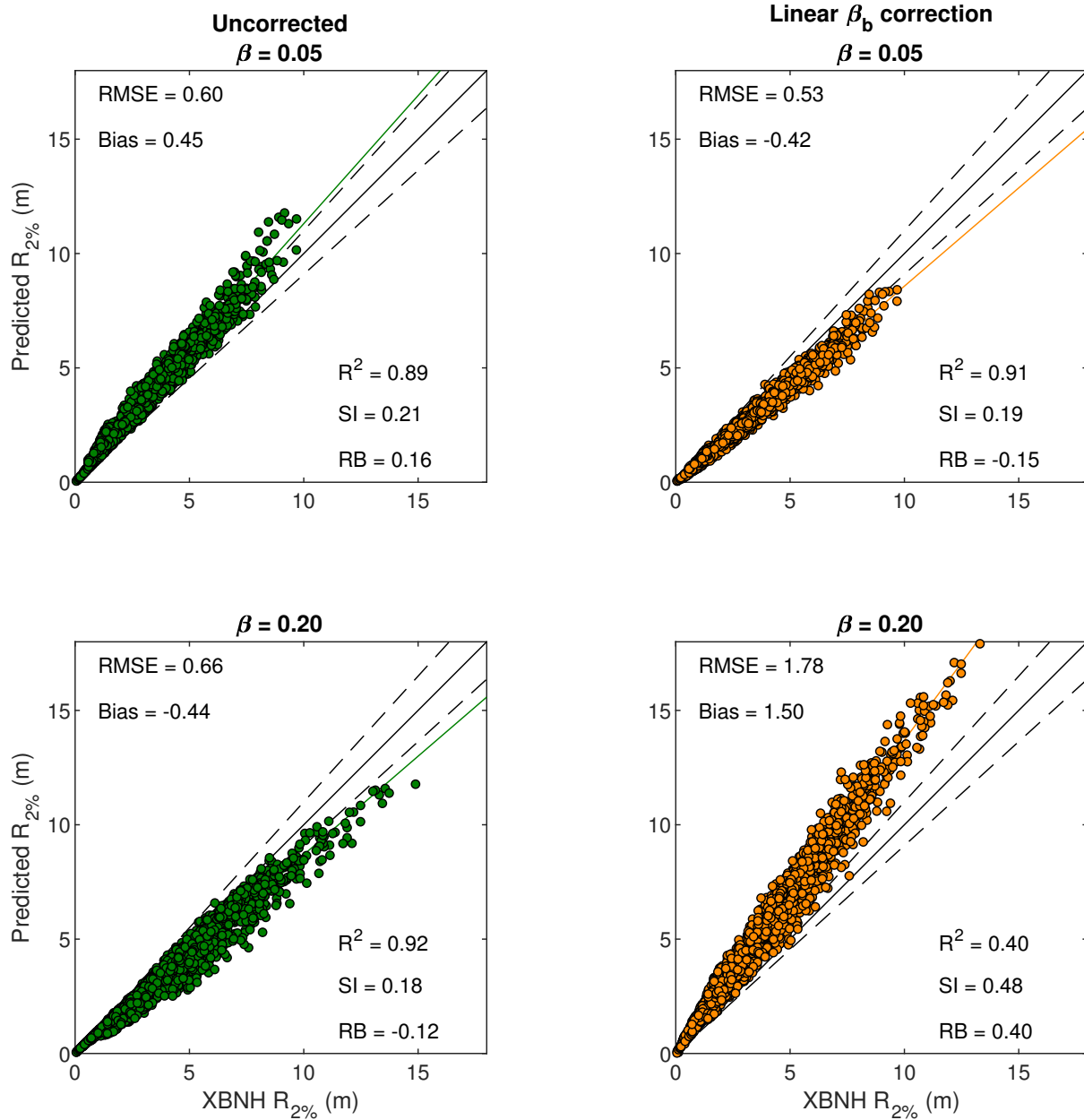
Figure A4. Wave runup predicted by BEWARE-2 relative to simulated by XBNH for milder (top panels) and steeper (bottom panels) beach slopes than the reference beach slope ($\beta_{b,\mathrm{ref}} = 0.10$) in the calibration dataset. Predictions are without beach slope correction (left panels) and with a correction factor α_b linearly proportional to β_b ($\kappa_b = 1$). Note the detrimental effect of the linear beach slope correction on the model skill in the bottom-right panel.
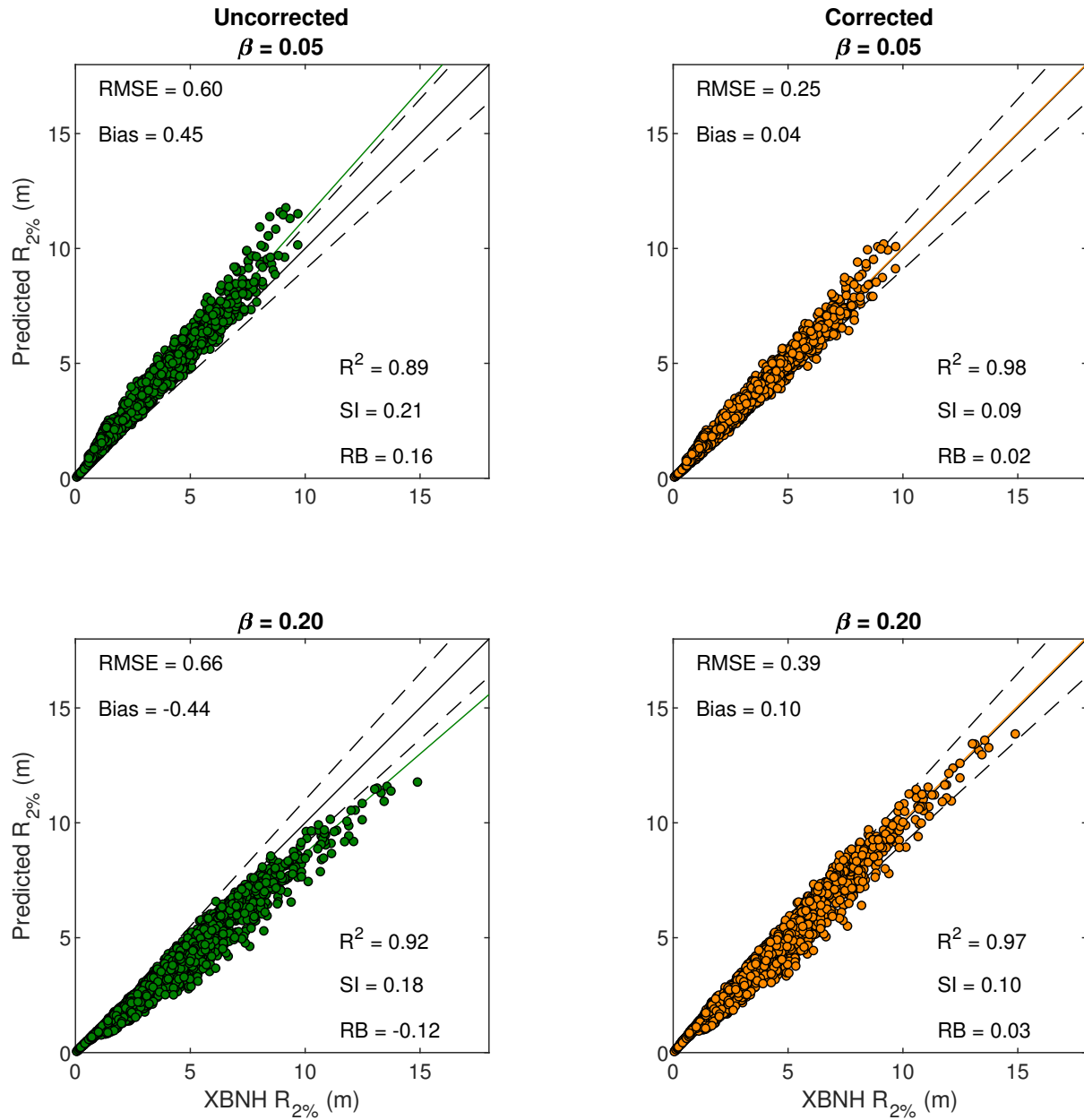
Figure A5. Wave runup predicted by BEWARE-2 relative to simulated by XBNH for milder (top panels) and steeper (bottom panels) beach slopes than the reference beach slope ($\beta_{b,\text{ref}} = 0.10$) in the calibration dataset using $\kappa_b = \frac{1}{e}$.

Author contributions. RM, CS, SP, and JA formulated the overall research aims and methodology; RM, FR, SP, JA, and RdG developed the BEWARE-2 software; CS provided data and supervised BEWARE-2 development; JA and FR extended the probabilistic profile matching methodology; RM developed the reef roughness and beach slope correction factors; FR and RdG prepared the training and validation data; RM, CS, and FR prepared the draft manuscript; SP and JA reviewed and edited the manuscript.

Competing interests. The authors declare that they have no conflict of interest.

Disclaimer. Any use of trade, firm, or product names is for descriptive purposes only and does not imply endorsement by the US Government.

Acknowledgements. This research was funded by the U.S. Geological Survey's Coastal and Marine Hazards and Resources Program and Deltares' Strategic Research in the Natural Hazards Program (11209194). We would like to thank Dr. M. Palmsten and Dr. B. Tsai for their suggestions and constructive review prior to submission to this journal.

	N_{match} (-)	p_{max} (%)	RMSE (m)	Bias (m)	SI (-)	RB (-)	R^2 (-)
AmSamoa: 5%	4	80	0.78	-0.06	0.08	-0.01	0.98
AmSamoa: 25%	6	35	0.44	0.14	0.05	0.02	0.99
AmSamoa: 50%	10	27	0.51	0.31	0.08	0.05	0.96
AmSamoa: 75%	10	25	0.75	0.66	0.16	0.14	0.83
AmSamoa: 95%	4	60	0.59	0.51	0.16	0.14	0.73
AmSamoa W	6	91	1.17	1.01	0.35	0.30	0.01
Florida: 5%	7	58	0.41	-0.17	0.09	-0.04	0.93
Florida: 25%	4	68	0.31	0.15	0.08	0.04	0.95
Florida: 50%	4	48	0.30	0.04	0.08	0.01	0.95
Florida: 75%	4	87	0.38	0.26	0.13	0.09	0.87
Florida: 95%	4	92	0.37	0.30	0.15	0.12	0.87
Florida W: 25%	5	87	0.34	0.21	0.11	0.07	0.90
Florida W: 75%	3	70	0.39	-0.20	0.24	-0.12	0.75
Guam: 5%	6	49	0.51	-0.00	0.06	-0.00	0.99
Guam: 25%	10	40	0.61	0.44	0.09	0.07	0.95
Guam: 50%	10	36	0.81	0.72	0.16	0.14	0.82
Guam: 75%	7	38	0.54	0.46	0.16	0.14	0.79
Guam: 95%	4	56	0.43	0.29	0.17	0.11	0.80
Guam W: 25%	3	98	0.43	0.13	0.18	0.05	0.79
Guam W: 75%	4	53	0.25	-0.18	0.12	-0.08	0.89
Hawaii: 5%	4	76	0.63	0.06	0.06	0.01	0.98
Hawaii: 25%	9	50	0.66	0.42	0.09	0.06	0.96
Hawaii: 50%	8	42	0.46	-0.18	0.09	-0.03	0.95
Hawaii: 75%	4	64	0.44	0.35	0.12	0.10	0.89
Hawaii: 95%	4	85	0.61	0.52	0.21	0.18	0.64
Hawaii W: 25%	7	56	0.33	-0.17	0.10	-0.05	0.92
Hawaii W: 75%	4	85	1.16	1.02	0.43	0.37	-0.53
PuertoRico: 5%	8	54	0.68	0.30	0.09	0.04	0.96
PuertoRico: 25%	10	37	0.63	0.52	0.11	0.09	0.93
PuertoRico: 50%	7	43	0.93	0.75	0.18	0.14	0.76
PuertoRico: 75%	7	29	0.44	0.32	0.11	0.08	0.88
PuertoRico: 95%	4	87	0.47	0.39	0.15	0.13	0.84
PuertoRico W: 25%	5	79	1.17	-0.81	0.23	-0.16	0.70
PuertoRico W: 75%	4	80	0.32	-0.10	0.08	-0.03	0.95
SaipanTinian: 5%	4	83	0.78	-0.05	0.08	-0.01	0.98
SaipanTinian: 25%	7	38	0.47	-0.02	0.05	-0.00	0.99
SaipanTinian: 50%	10	46	0.80	0.62	0.12	0.09	0.92
SaipanTinian: 75%	10	30	0.73	0.61	0.14	0.12	0.89
SaipanTinian: 95%	4	93	0.19	0.06	0.08	0.02	0.97
SaipanTinian W: 25%	4	94	0.51	-0.10	0.20	-0.04	0.78
SaipanTinian W: 75%	4	74	1.16	1.00	0.39	0.34	-0.25
USVI: 5%	6	59	0.56	0.03	0.06	0.00	0.99
USVI: 25%	8	42	0.42	-0.08	0.06	-0.01	0.98
USVI: 50%	6	64	0.42	0.20	0.07	0.04	0.97
USVI: 75%	4	89	0.41	0.23	0.09	0.05	0.94
USVI: 95%	6	87	0.24	0.12	0.08	0.04	0.95
USVI W: 25%	4	96	0.53	0.24	0.14	0.06	0.88
USVI W: 75%	9	50	0.44	0.38	0.17	0.15	0.74

Table A1. Overview of profile matching properties and model skill values for the 48 validation profiles. Matching properties include the number of probabilistically matched RRPs (N_{match}) and the maximum matching probability (p_{max}), and skill values include the root-mean-square error (RMSE), model bias (Bias), scatter index (SI), relative bias (RB), and coefficient of determination (R^2) of the BEWARE-2 wave runup prediction.

References

Albert, S., Leon, J. X., Grinham, A. R., Church, J. A., Gibbes, B. R., and Woodroffe, C. D.: Interactions between sea-level rise and wave exposure on reef island dynamics in the Solomon Islands, Environmental Research Letters, 11, 054 011, https://doi.org/10.1088/1748-9326/11/5/054011, publisher: IOP Publishing, 2016.

Astorga-Moar, A. and Baldock, T. E.: Assessment of wave overtopping models for fringing reef fronted beaches., Coastal Engineering, 186, 104 395, https://doi.org/10.1016/j.coastaleng.2023.104395, 2023.

Bakker, T. M., Antolínez, J. A. A., Leijnse, T. W. B., Pearson, S. G., and Giardino, A.: Estimating tropical cyclone-induced wind, waves, and surge: A general methodology based on representative tracks, Coastal Engineering, 176, 104 154, https://doi.org/10.1016/j.coastaleng.2022.104154, 2022.

Beck, M. W., Losada, I. J., Menéndez, P., Reguero, B. G., Díaz-Simal, P., and Fernández, F.: The global flood protection savings provided by coral reefs, Nature Communications, 9, 2186, https://doi.org/10.1038/s41467-018-04568-z, number: 1 Publisher: Nature Publishing Group, 2018.

Beetham, E. and Kench, P. S.: Predicting wave overtopping thresholds on coral reef-island shorelines with future sea-level rise, Nature Communications, 9, 3997, https://doi.org/10.1038/s41467-018-06550-1, publisher: Nature Publishing Group, 2018.

Bridle, J. S.: Probabilistic Interpretation of Feedforward Classification Network Outputs, with Relationships to Statistical Pattern Recognition, in: Neurocomputing, edited by Soulié, F. F. and Hérault, J., NATO ASI Series, pp. 227–236, Springer, Berlin, Heidelberg, ISBN 978-3-642-76153-9, https://doi.org/10.1007/978-3-642-76153-9_28, 1990.

Buckley, M. L., Lowe, R. J., Hansen, J. E., van Dongeren, A. R., and Storlazzi, C. D.: Mechanisms of Wave-Driven Water Level Variability on Reef-Fringed Coastlines, Journal of Geophysical Research: Oceans, 123, 3811–3831, https://doi.org/10.1029/2018JC013933, _eprint: https://onlinelibrary.wiley.com/doi/pdf/10.1029/2018JC013933, 2018.

Cheriton, O. M., Storlazzi, C. D., and Rosenberger, K. J.: Observations of wave transformation over a fringing coral reef and the importance of low-frequency waves and offshore water levels to runup, overwash, and coastal flooding, Journal of Geophysical Research: Oceans, 121, 3121–3140, https://doi.org/10.1002/2015JC011231, _eprint: https://onlinelibrary.wiley.com/doi/pdf/10.1002/2015JC011231, 2016.

Chilunga, F. P., Rodriguez-Llanes, J. M., and Guha-Sapir, D.: Rapid Urbanization is Linked to Flood Lethality in the Small Island Developing States (SIDS): A Modeling Study, Prehospital and Disaster Medicine, 32, S190–S190, https://doi.org/10.1017/S1049023X17005015, publisher: Cambridge University Press, 2017.

Coz, J., Alsheimer, F., and Lindner, B. L.: A Climatology-Based Forecast Tool for Coastal Flooding in the Low Country, Journal of Applied Meteorology and Climatology, 60, 893–908, https://doi.org/10.1175/JAMC-D-20-0256.1, publisher: American Meteorological Society Section: Journal of Applied Meteorology and Climatology, 2021.

de Beer, A. F., McCall, R. T., Long, J. W., Tissier, M. F. S., and Reniers, A. J. H. M.: Simulating wave runup on an intermediate–reflective beach using a wave-resolving and a wave-averaged version of XBeach, Coastal Engineering, 163, 103 788, https://doi.org/10.1016/j.coastaleng.2020.103788, 2021.

de Ridder, M. P., Smit, P. B., van Dongeren, A. R., McCall, R. T., Nederhoff, K., and Reniers, A. J. H. M.: Efficient two-layer non-hydrostatic wave model with accurate dispersive behaviour, Coastal Engineering, 164, 103 808, https://doi.org/10.1016/j.coastaleng.2020.103808, 2021.

Doong, D.-J., Chuang, L. Z.-H., Wu, L.-C., Fan, Y.-M., Kao, C. C., and Wang, J.-H.: Development of an operational coastal flooding early warning system, Natural Hazards and Earth System Sciences, 12, 379–390, https://doi.org/10.5194/nhess-12-379-2012, publisher:
700   Copernicus GmbH, 2012.

Egbert, G. D. and Erofeeva, S. Y.: Efficient Inverse Modeling of Barotropic Ocean Tides, Journal of Atmospheric and Oceanic Technology, 19, 183–204, https://doi.org/10.1175/1520-0426(2002)019<0183:EIMOBO>2.0.CO;2, publisher: American Meteorological Society Section: Journal of Atmospheric and Oceanic Technology, 2002.

Ford, M., Merrifield, M. A., and Becker, J. M.: Inundation of a low-lying urban atoll island: Majuro, Marshall Islands, Natural Hazards, 91,
705   1273–1297, https://doi.org/10.1007/s11069-018-3183-5, 2018.

Franklin, G. L. and Torres-Freyermuth, A.: On the runup parameterisation for reef-lined coasts, Ocean Modelling, 169, 101 929, https://doi.org/10.1016/j.ocemod.2021.101929, 2022.

Gawehn, M., van Dongeren, A., van Rooijen, A., Storlazzi, C. D., Cheriton, O. M., and Reniers, A.: Identification and classification of very low frequency waves on a coral reef flat, Journal of Geophysical Research: Oceans, 121, 7560–7574,
710   https://doi.org/10.1002/2016JC011834, _eprint: https://onlinelibrary.wiley.com/doi/pdf/10.1002/2016JC011834, 2016.

Halliwell, G., Bleck, R., and Chassignet, E.: Atlantic Ocean simulations performed using a new hybrid-coordinate ocean model, in: EOS Proceedings of AGU Fall Meeting, 1998.

Harris, D. L., Rovere, A., Casella, E., Power, H., Canavesio, R., Collin, A., Pomeroy, A., Webster, J. M., and Parravicini, V.: Coral reef structural complexity provides important coastal protection from waves under rising sea levels, Science Advances, 4, eaao4350,
715   https://doi.org/10.1126/sciadv.aao4350, publisher: American Association for the Advancement of Science, 2018.

Hasselmann, K., Barnett, T. P., Bouws, E., Carlson, H., Cartwright, D. E., Enke, K., Ewing, J. A., Gienapp, A., Hasselmann, D. E., Kruseman, P., Meerburg, A., Müller, P., Olbers, D. J., Richter, K., Sell, W., and Walden, H.: Measurements of wind-wave growth and swell decay during the joint North Sea wave project (JONSWAP)., Ergänzungsheft zur Deutschen Hydrographischen Zeitschrift, Reihe A, Nr. 12, https://pure.mpg.de/pubman/faces/ViewItemOverviewPage.jsp?itemId=item_3262854, 1973.

720   Hinkel, J., Lincke, D., Vafeidis, A. T., Perrette, M., Nicholls, R. J., Tol, R. S. J., Marzeion, B., Fettweis, X., Ionescu, C., and Levermann, A.: Coastal flood damage and adaptation costs under 21st century sea-level rise, Proceedings of the National Academy of Sciences, 111, 3292–3297, https://doi.org/10.1073/pnas.1222469111, publisher: Proceedings of the National Academy of Sciences, 2014.

Hoeke, R. K., McInnes, K. L., Kruger, J. C., McNaught, R. J., Hunter, J. R., and Smithers, S. G.: Widespread inundation of Pacific islands triggered by distant-source wind-waves, Global and Planetary Change, 108, 128–138, https://doi.org/10.1016/j.gloplacha.2013.06.006,
725   2013.

Hoeke, R. K., Damlamian, H., Aucan, J., and Wandres, M.: Severe Flooding in the Atoll Nations of Tuvalu and Kiribati Triggered by a Distant Tropical Cyclone Pam, Frontiers in Marine Science, 7, https://doi.org/10.3389/fmars.2020.539646, publisher: Frontiers, 2021.

Holman, R. A. and Stanley, J.: The history and technical capabilities of Argus, Coastal Engineering, 54, 477–491, https://doi.org/10.1016/j.coastaleng.2007.01.003, 2007.

730   Klaver, S., Nederhoff, C. M., Giardino, A., Tissier, M. F. S., van Dongeren, A. R., and van der Spek, A. J. F.: Impact of Coral Reef Mining Pits on Nearshore Hydrodynamics and Wave Runup During Extreme Wave Events, Journal of Geophysical Research: Oceans, 124, 2824–2841, https://doi.org/10.1029/2018JC014165, _eprint: https://onlinelibrary.wiley.com/doi/pdf/10.1029/2018JC014165, 2019.

Kumar, L. and Taylor, S.: Exposure of coastal built assets in the South Pacific to climate risks, Nature Climate Change, 5, 992–996, https://doi.org/10.1038/nclimate2702, number: 11 Publisher: Nature Publishing Group, 2015.

735   Laigre, T., Balouin, Y., Villarroel-Lamb, D., Lerma, A. N., Valentini, N., Moisan, M., and De La Torre, Y.: Total Water Level Mitigation Related to Fringing Reef and Upperbeach Vegetation Status at a Hurricane Exposed Coast, Journal of Marine Science and Engineering, 11, 620, https://doi.org/10.3390/jmse11030620, number: 3 Publisher: Multidisciplinary Digital Publishing Institute, 2023.

Lashley, C. H., Roelvink, D., van Dongeren, A., Buckley, M. L., and Lowe, R. J.: Nonhydrostatic and surfbeat model predictions of extreme wave run-up in fringing reef environments, Coastal Engineering, 137, 11–27, https://doi.org/10.1016/j.coastaleng.2018.03.007, 2018.

740   Liu, Y., Li, S., Liao, Z., Liu, Q., Zou, Q., and Liu, W.: Explicit wave-runup formula for beaches fronted by coral reefs using tree-based models, Coastal Engineering, 183, 104 308, https://doi.org/10.1016/j.coastaleng.2023.104308, 2023.

Lowe, R. J., Falter, J. L., Bandet, M. D., Pawlak, G., Atkinson, M. J., Monismith, S. G., and Koseff, J. R.: Spectral wave dissipation over a barrier reef, Journal of Geophysical Research: Oceans, 110, https://doi.org/10.1029/2004JC002711, _eprint: https://onlinelibrary.wiley.com/doi/pdf/10.1029/2004JC002711, 2005.

745   Masselink, G., Tuck, M., McCall, R., van Dongeren, A., Ford, M., and Kench, P.: Physical and Numerical Modeling of Infragravity Wave Generation and Transformation on Coral Reef Platforms, Journal of Geophysical Research: Oceans, 124, 1410–1433, https://doi.org/10.1029/2018JC014411, _eprint: https://onlinelibrary.wiley.com/doi/pdf/10.1029/2018JC014411, 2019.

Masselink, G., Beetham, E., and Kench, P.: Coral reef islands can accrete vertically in response to sea level rise, Science Advances, 6, eaay3656, https://doi.org/10.1126/sciadv.aay3656, publisher: American Association for the Advancement of Science, 2020.

750   Masselink, G., McCall, R., Beetham, E., Kench, P., and Storlazzi, C.: Role of Future Reef Growth on Morphological Response of Coral Reef Islands to Sea-Level Rise, Journal of Geophysical Research: Earth Surface, 126, e2020JF005 749, https://doi.org/10.1029/2020JF005749, _eprint: https://onlinelibrary.wiley.com/doi/pdf/10.1029/2020JF005749, 2021.

Melter, R. A.: Some characterizations of city block distance, Pattern Recognition Letters, 6, 235–240, https://doi.org/10.1016/0167-8655(87)90082-1, 1987.

755   Merrifield, M. A., Becker, J. M., Ford, M., and Yao, Y.: Observations and estimates of wave-driven water level extremes at the Marshall Islands, Geophysical Research Letters, 41, 7245–7253, https://doi.org/10.1002/2014GL061005, _eprint: https://onlinelibrary.wiley.com/doi/pdf/10.1002/2014GL061005, 2014.

Monismith, S. G., Herdman, L. M. M., Ahmerkamp, S., and Hench, J. L.: Wave Transformation and Wave-Driven Flow across a Steep Coral Reef, Journal of Physical Oceanography, 43, 1356–1379, https://doi.org/10.1175/JPO-D-12-0164.1, publisher: American Meteorological
760   Society Section: Journal of Physical Oceanography, 2013.

Norris, B. K., Storlazzi, C. D., Pomeroy, A. W. M., Rosenberger, K. J., Logan, J. B., and Cheriton, O. M.: Combining field observations and high-resolution numerical modeling to demonstrate the effect of coral reef roughness on turbulence and its implications for reef restoration design, Coastal Engineering, 184, 104 331, https://doi.org/10.1016/j.coastaleng.2023.104331, 2023.

Pearson, S. G., Storlazzi, C. D., van Dongeren, A. R., Tissier, M. F. S., and Reniers, A. J. H. M.: A Bayesian-Based System to As-
765   sess Wave-Driven Flooding Hazards on Coral Reef-Lined Coasts, Journal of Geophysical Research: Oceans, 122, 10 099–10 117, https://doi.org/10.1002/2017JC013204, _eprint: https://onlinelibrary.wiley.com/doi/pdf/10.1002/2017JC013204, 2017.

Pomeroy, A. and van Rooijen, A.: The impact of fringing platform reefs on shoreline profiles, in: Proceedings of Australasian Coasts and Ports 2019 Conference, Hobart, Tasmania, Australia, 2019.

Pomeroy, A., Lowe, R., Symonds, G., Van Dongeren, A., and Moore, C.: The dynamics of infragravity wave transfor-
770   mation over a fringing reef, Journal of Geophysical Research: Oceans, 117, https://doi.org/10.1029/2012JC008310, _eprint: https://onlinelibrary.wiley.com/doi/pdf/10.1029/2012JC008310, 2012.

Péquignet, A. C. N., Becker, J. M., Merrifield, M. A., and Aucan, J.: Forcing of resonant modes on a fringing reef during tropical storm Man-Yi, Geophysical Research Letters, 36, https://doi.org/10.1029/2008GL036259, _eprint: https://onlinelibrary.wiley.com/doi/pdf/10.1029/2008GL036259, 2009.

775 Péquignet, A.-C. N., Becker, J. M., and Merrifield, M. A.: Energy transfer between wind waves and low-frequency oscillations on a fringing reef, Ipan, Guam, Journal of Geophysical Research: Oceans, 119, 6709–6724, https://doi.org/10.1002/2014JC010179, _eprint: https://onlinelibrary.wiley.com/doi/pdf/10.1002/2014JC010179, 2014.

Quataert, E., Storlazzi, C., van Rooijen, A., Cheriton, O., and van Dongeren, A.: The influence of coral reefs and climate change on wave-driven flooding of tropical coastlines, Geophysical Research Letters, 42, 6407–6415, https://doi.org/10.1002/2015GL064861, _eprint:
780 https://onlinelibrary.wiley.com/doi/pdf/10.1002/2015GL064861, 2015.

Quataert, E., Storlazzi, C., van Dongeren, A., and McCall, R.: The importance of explicitly modelling sea-swell waves for runup on reef-lined coasts, Coastal Engineering, 160, 103 704, https://doi.org/10.1016/j.coastaleng.2020.103704, 2020.

Reynolds, M. H., Courtot, K. N., Berkowitz, P., Storlazzi, C. D., Moore, J., and Flint, E.: Will the Effects of Sea-Level Rise Create Ecological Traps for Pacific Island Seabirds?, PLOS ONE, 10, e0136 773, https://doi.org/10.1371/journal.pone.0136773, publisher: Public Library of
785 Science, 2015.

Roeber, V. and Bricker, J. D.: Destructive tsunami-like wave generated by surf beat over a coral reef during Typhoon Haiyan, Nature Communications, 6, 7854, https://doi.org/10.1038/ncomms8854, number: 1 Publisher: Nature Publishing Group, 2015.

Roelvink, D., Reniers, A., van Dongeren, A., van Thiel de Vries, J., McCall, R., and Lescinski, J.: Modelling storm impacts on beaches, dunes and barrier islands, Coastal Engineering, 56, 1133–1152, https://doi.org/10.1016/j.coastaleng.2009.08.006, 2009.

790 Roelvink, D., McCall, R., Mehvar, S., Nederhoff, K., and Dastgheib, A.: Improving predictions of swash dynamics in XBeach: The role of groupiness and incident-band runup, Coastal Engineering, 134, 103–123, https://doi.org/10.1016/j.coastaleng.2017.07.004, 2018.

Roelvink, F. E., Storlazzi, C. D., van Dongeren, A. R., and Pearson, S. G.: Coral Reef Restorations Can Be Optimized to Reduce Coastal Flooding Hazards, Frontiers in Marine Science, 8, https://www.frontiersin.org/articles/10.3389/fmars.2021.653945, 2021.

Rueda, A., Cagigal, L., Pearson, S., Antolínez, J. A. A., Storlazzi, C., van Dongeren, A., Camus, P., and Mendez, F. J.: HyCReWW: A Hybrid
795 Coral Reef Wave and Water level metamodel, Computers & Geosciences, 127, 85–90, https://doi.org/10.1016/j.cageo.2019.03.004, 2019.

Scott, F., Antolinez, J. A. A., McCall, R., Storlazzi, C., Reniers, A., and Pearson, S.: Hydro-Morphological Characterization of Coral Reefs for Wave Runup Prediction, Frontiers in Marine Science, 7, https://www.frontiersin.org/articles/10.3389/fmars.2020.00361, 2020.

Shimozono, T., Tajima, Y., Kennedy, A. B., Nobuoka, H., Sasaki, J., and Sato, S.: Combined infragravity wave and sea-swell runup over fringing reefs by super typhoon Haiyan, Journal of Geophysical Research: Oceans, 120, 4463–4486, https://doi.org/10.1002/2015JC010760,
800 _eprint: https://onlinelibrary.wiley.com/doi/pdf/10.1002/2015JC010760, 2015.

Sing Wong, A., Vrontos, S., and Taylor, M. L.: An assessment of people living by coral reefs over space and time, Global Change Biology, 28, 7139–7153, https://doi.org/10.1111/gcb.16391, _eprint: https://onlinelibrary.wiley.com/doi/pdf/10.1111/gcb.16391, 2022.

Smit, P., Stelling, G., Roelvink, D. J., Thiel de Vries, J., McCall, R., van Dongeren, A., Zwinkels, C., and Jacobs, R.: XBeach: Non-hydrostatic model: Validation, verification and model description, Tech. rep., Delft University of Technology, 2010.

805 Stockdon, H. F., Holman, R. A., Howd, P. A., and Sallenger, A. H.: Empirical parameterization of setup, swash, and runup, Coastal Engineering, 53, 573–588, https://doi.org/10.1016/j.coastaleng.2005.12.005, 2006.

Stockdon, H. F., Long, J. W., Palmsten, M. L., Van der Westhuysen, A., Doran, K. S., and Snell, R. J.: Operational forecasts of wave-driven water levels and coastal hazards for US Gulf and Atlantic coasts, Communications Earth & Environment, 4, 1–8, https://doi.org/10.1038/s43247-023-00817-2, number: 1 Publisher: Nature Publishing Group, 2023.

810 Storlazzi, C. D., Gingerich, S. B., van Dongeren, A., Cheriton, O. M., Swarzenski, P. W., Quataert, E., Voss, C. I., Field, D. W., Annamalai, H., Piniak, G. A., and McCall, R.: Most atolls will be uninhabitable by the mid-21st century because of sea-level rise exacerbating wave-driven flooding, Science Advances, 4, eaap9741, https://doi.org/10.1126/sciadv.aap9741, publisher: American Association for the Advancement of Science, 2018.

Storlazzi, C. D., Reguero, B. G., Cole, A. D., Lowe, E., Shope, J. B., Gibbs, A. E., Nickel, B. A., McCall, R. T., Dongeren, A. R. v., and Beck,
815 M. W.: Rigorously valuing the role of U.S. coral reefs in coastal hazard risk reduction, Tech. Rep. 2019-1027, U.S. Geological Survey, https://doi.org/10.3133/ofr20191027, iSSN: 2331-1258 Publication Title: Open-File Report, 2019.

Storlazzi, C. D., Rey, A. E., and van Dongeren, A. R.: A Numerical Study of Geomorphic and Oceanographic Controls on Wave-Driven Runup on Fringing Reefs with Shore-Normal Channels, Journal of Marine Science and Engineering, 10, 828, https://doi.org/10.3390/jmse10060828, number: 6 Publisher: Multidisciplinary Digital Publishing Institute, 2022.

820 Symonds, G., Huntley, D. A., and Bowen, A. J.: Two-dimensional surf beat: Long wave generation by a time-varying breakpoint, Journal of Geophysical Research: Oceans, 87, 492–498, https://doi.org/10.1029/JC087iC01p00492, _eprint: https://onlinelibrary.wiley.com/doi/pdf/10.1029/JC087iC01p00492, 1982.

Tolman, H. L.: User manual and system documentation of WAVEWATCH III TM version 3.14, Technical Note MMAB Contribution No. 276, National Oceanic and Atmospheric Administration, 2009.

825 UNISDR: Sendai Framework for Disaster Risk Reduction 2015 - 2030, Tech. rep., 2015.

Van Dongeren, A., Lowe, R., Pomeroy, A., Trang, D. M., Roelvink, D., Symonds, G., and Ranasinghe, R.: Numerical modeling of low-frequency wave dynamics over a fringing coral reef, Coastal Engineering, 73, 178–190, https://doi.org/10.1016/j.coastaleng.2012.11.004, 2013.

Vitousek, S., Barnard, P. L., Fletcher, C. H., Frazer, N., Erikson, L., and Storlazzi, C. D.: Doubling of coastal flooding frequency within
830 decades due to sea-level rise, Scientific Reports, 7, 1399, https://doi.org/10.1038/s41598-017-01362-7, 2017.

Vousdoukas, M. I., Mentaschi, L., Voukouvalas, E., Verlaan, M., Jevrejeva, S., Jackson, L. P., and Feyen, L.: Global probabilistic projections of extreme sea levels show intensification of coastal flood hazard, Nature Communications, 9, 2360, https://doi.org/10.1038/s41467-018-04692-w, number: 1 Publisher: Nature Publishing Group, 2018.

Wadey, M., Brown, S., Nicholls, R. J., and Haigh, I.: Coastal flooding in the Maldives: an assessment of historic events and their implications,
835 Natural Hazards, 89, 131–159, https://doi.org/10.1007/s11069-017-2957-5, 2017.

Wandres, M., Aucan, J., Espejo, A., Jackson, N., De Ramon N'Yeurt, A., and Damlamian, H.: Distant-Source Swells Cause Coastal Inundation on Fiji's Coral Coast, Frontiers in Marine Science, 7, https://doi.org/10.3389/fmars.2020.00546, publisher: Frontiers, 2020.

Winter, G., Storlazzi, C., Vitousek, S., van Dongeren, A., McCall, R., Hoeke, R., Skirving, W., Marra, J., Reyns, J., Aucan, J., Widlansky, M., Becker, J., Perry, C., Masselink, G., Lowe, R., Ford, M., Pomeroy, A., Mendez, F., Rueda, A., and Wandres, M.: Steps to Develop Early
840 Warning Systems and Future Scenarios of Storm Wave-Driven Flooding Along Coral Reef-Lined Coasts, Frontiers in Marine Science, 7, https://www.frontiersin.org/articles/10.3389/fmars.2020.00199, 2020.

WMO: Early Warnings for All: The UN Global Early Warning Initiative for the Implementation of Climate Adaptation. Executive Action Plan 2023–2027, https://library.wmo.int/idurl/4/58209, 2022a.

WMO: Guidelines on Implementation of a Coastal Inundation Forecasting–Early Warning System, Tech. Rep. WMO-No. 1293, 2022b.